View Article Online
View Journal

Environmental Science Nano

Accepted Manuscript

This article can be cited before page numbers have been issued, to do this please use: Z. Wang, A. Pilechi and P. Ariya, *Environ. Sci.: Nano*, 2026, DOI: 10.1039/D5EN01084E.

ROYAL SOCIETY OF CHEMISTRY

rsc.li/es-nano

View Article Online
DOI: 10.1039/D5EN01084E

Environmental Significance Statement

Nanoplastics are an emerging contaminant of global concern, yet their detection in water remains hindered by their nanoscale dimensions, diverse chemistries, and interactions with natural matrices. While microplastics have been more extensively studied, this review places particular emphasis on nanoplastics, whose environmental monitoring remains scarce. We examine recent advances in analytical methods, spanning spectroscopy, mass spectrometry, laser-based imaging, holographic microscopy, and microfluidic platforms, and highlight the growing use of artificial intelligence for automated detection and classification. We further explore how integrating analytical approaches and field measurements with modelling can enhance predictive capacity and feedback into method development. Together, these advances enable more accurate exposure assessments, strengthen risk evaluation, and provide the foundation for effective policy responses to plastic pollution.

View Article Online
DOI: 10.1039/D5EN01084E

Waterborne Nanoplastics and Microplastics: Analytical Advances, Modelling, and Future Directions

Zi Wang[1], Abolghasem Pilechi[2], and Parisa A. Ariya[1, 3, *]

[1]Department of Chemistry, McGill University, Montreal, Quebec, H3A 0B8, Canada; [2]National Research Council Canada, Ottawa, Ontario, K1A 0R6, Canada; [3]Department of Atmospheric and Oceanic Sciences, McGill University, Montreal, Quebec, H3A 0B9, Canada

*Corresponding to: parisa.ariya@mcgill.ca

Abstract

Plastics' persistence throughout their life cycle has imposed a global burden of nano- and microplastics in aquatic systems. This Frontier Review consolidates recent advances in analytics, machine learning, and fate and transport modelling, and sets a practical agenda for decision-ready measurements. Analytical breakthroughs enable chemically specific imaging at tens-of-nanometre resolution using sub-micron vibrational methods, while hyperspectral stimulated Raman scattering delivers rapid single-particle chemical mapping. Emerging holography techniques provide in-situ, real-time physicochemical characterization, capturing 3D size, shape, surface coatings, and other features and can distinguish nano- and microplastics from other particles within milliseconds. Complementary innovations, including label-free photonic and electrochemical sensors and separation workflows coupled with mass spectrometry, extend polymer specificity and quantification in complex waters. Across these platforms, machine learning accelerates denoising, feature extraction, automated classification, and imaging throughput. Yet, performance remains constrained by biased or limited datasets, label noise, and domain shifts across instruments, matrices, and weathering states. Modelling frontiers require adaptation for nanoplastics, where Brownian diffusion, rapid aggregation, and dynamic eco-coronas govern transport and water–sediment exchange. Existing nanomaterial models offer transferable scaffolds when re-parameterized for nanoplastic behaviour. To enable interoperable, validated, and scalable systems, we recommend:

View Article Online
DOI: 10.1039/D5EN01084E

(a) universal Report Nano- and Microplastic Analytics checklist aligned with International Organization for Standardization (ISO) guidance for diverse media; (b) standard reference materials and blinded interlaboratory trials; (c) open, versioned datasets; (d) machine learning tasks with fixed splits and uncertainty reporting; (e) routine, end-to-end uncertainty quantification and traceability; (f) field testbeds integrating sensors, analytics, and fate and transport models to deliver policy-relevant indicators with calibrated confidence. Together, these steps will transform fragmented efforts into robust, decision-ready frameworks for safeguarding water quality in the age of nanoplastics.

1. Introduction

Plastics originated in 1862 when Alexandre Parkes patented the first artificial plastic, derived from cellulose, a natural polymer [1]. Within a few years, numerous scientists and inventors became interested in this material, sparking a revolution that transformed everyday life, from food packaging and medicine to electronics. Plastics enabled the mass production of lightweight, durable products across diverse sectors. While plastics have undeniably reshaped modern living, their persistence throughout production, use, and disposal has created a long-lasting pollution burden that now affects nearly every environmental compartment.

Every year, an estimated 19 to 23 million tonnes of plastic waste leak into aquatic ecosystems, polluting lakes, rivers, and seas [2]. Global plastics production and waste are projected to increase through mid-century in the absence of stronger policy action, with leakage to aquatic systems expected to continue even under ambitious mitigation scenarios [3, 4]. These trends align with ongoing negotiations on a legally binding treaty to end plastic pollution, highlighting the need for actionable science to guide mitigation across the entire life cycle of plastics [5].

While microplastics have received considerable attention, research is increasingly shifting toward smaller and analytically more challenging nanoplastics. Owing to their substantially higher surface area, distinct colloidal behaviour, and ability to traverse biological barriers more readily than larger particles, nanoplastics necessitate specialized analytical and modelling approaches. Recent standardization efforts (e.g., ISO

View Article Online
DOI: 10.1039/D5EN01084E

24187:2023) has begun harmonizing microplastic terminology, facilitating cross-study comparisons [6-8]. Consequently, most current studies adopt an operational definition of nanoplastics as particles < 1 μm, consistent with instrumental detection limits and colloidal properties [6, 9, 10].

Analytical advances over the past few years are reshaping what can be measured in laboratories environmental matrices. Submicron techniques such as optical photothermal infrared (O-PTIR) and atomic force microscopy-infrared spectroscopy (AFM-IR) have extended chemically specific imaging into the hundreds of nanometres regime, and in some cases down to tens of nanometres [11, 12]. Field-relevant demonstrations show that coupled O-PTIR and AFM-IR can detect and map nanoplastics within snow and water samples [13, 14]. In parallel, hyperspectral stimulated Raman scattering (SRS) spectroscopy has emerged as a rapid single-particle platform for identifying nano- and microplastics. Analyses of bottled water have measured ~ 10^5 plastics·L^{-1}, ~ 90% of which are nanoplastics, markedly elevating prior intake estimates [15]. Table 1 summarizes representative analytical techniques commonly used for measuring waterborne nano- and microplastics in environmental samples.

Table 1 | A brief overview of commonly used technologies for nano- and microplastic detection in environmental waters. Selected mass-based and particle-based techniques for identification and quantification are tabulated, and their typical applications, key advantages, and main limitations are summarized for comparison.

Technologies	Major Applications	Key Strengths	Main Limitations	Examples	Ref.
Mass Spectrometry	*Py-GC-MS* • Polymer identification • Additives and oligomers • Mass-based quantification	• High chemical specificity (GC separation) • Complex matrices (with cleanup) • Relatively mature, widely adopted	• Destructive • Preparation and analysis can be slow • Marker, library, and matrix effects can bias	Identifying and quantifying PE, PP, PS, PET, PVC, and PMMA in surface water and riverside groundwater	[16, 17]
	TD-PTR-MS • Rapid screening of thermal desorption markers • High throughput comparisons • Process or aging proxies	• Relatively fast • Sensitive to VOC/SVOC markers • Time-resolved signal during heating	• Lower specificity (overlapping markers/isobars) • Quantification harder (calibration/transfer efficiency) • Destructive • Limited for low-volatility fractions	Identifying and quantifying PE, PP, PET, and PVC in lakes and streams	[18, 19]
	MALDI-TOF-MS • Oligomer or repeat unit patterns • Polymer-dependent MW distribution	• Fast spectra • Insight into MW and oligomer series • Not inherently limited by particle size	• Typically low throughput • Preparation sensitive (matrix and cation) • Molecular weight range constraints • Polymer-dependent ionization bias	Detecting PE and PTHF in lake and river waters	[20, 21]

Infrared Spectroscopy	*ATR-FTIR* • Identification of larger plastic particles/fragments • QA/QC checks for reference materials	• Simple, widely available • Relatively easy sample preparation • Polymer specificity for many common plastics • Easy to combine with complementary techniques	• Low throughput, one-at-a-time • Particle size limit • Surface contamination (e.g., biofilms) can interfere	Analyzing small microplastics in marine water samples	[22, 23]
	μ-FTIR (Micro-FTIR imaging / microspectroscopy) • Automated mapping and identification of particles on filters • Size distribution and counts (down to ~ 10 - 20 μm typical)	• Higher throughput than conventional ATR • Produces chemical maps and particle metrics • Standardizable filter-based workflows	• Still limited for nano range • Long scan times at high resolution • Spectral mixing, weathering/additives/biofilms can reduce match quality	Detection of 12 polymer types in 22 urban water samples	[24, 25]
	LDIR (Laser direct infrared / QCL-based IR imaging) • Rapid chemical imaging and identification of plastic particles on substrates • High throughput particle surveys	• Fast imaging (high throughput) • Automated particle detection and identification • Screening of particles	• Detection limit depends on optics/substrate • Susceptible to low SNR, thickness/substrate artifacts • Domain shift across instruments and matrices • Library and machine learning model dependence for classification	Detection of PE, PP, PS, and PVC in 7 groundwater bores	[26, 27]
Raman Spectroscopy	*SERS* • Trace level polymer/additive detection • Nanoplastic focused assays	• High sensitivity (signal enhancement) • Can work for very small/low-mass targets when adsorption is effective	• Strong dependence on substrate quality, hotspots, and particle-substrate contact (reproducibility) • Quantification difficult, signal varies spatially	Measuring the concentration of PS nanoplastics in a river water sample	[28, 29]

	• Hotspot-based mapping	• Fast spectra once captured	• Interference from fluorescence, organic coatings, and salts		
	μ-Raman (Micro-Raman microscopy / mapping) • Polymer ID • Particle counts/size on filters • Pigment and additive information, weathering signatures • Detailed single particle verification	• High chemical specificity with little sample preparation • Polymer identification at smaller particle sizes • Flexible point identification and mapping • Widely available	• Fluorescence can overwhelm spectra (biofilms/organics/dyes) • Slower throughput for large-area scans • Laser heating/photodegradation risk for some polymers • Focusing and substrate effects can bias results	Testing microplastic content in drinking water samples	[30, 31]
Fluorescence Spectroscopy / Microscopy	• Rapid screening and counting of suspected plastic particles • Size and shape mapping on filters • Bulk/spot fluorescence tracking (relative changes) • Pre-selection of particles for FTIR/Raman	• Fast, high throughput • Low cost, widely accessible • Good for locating small/faint particles	• Not polymer specific (needs FTIR/Raman/MS to confirm) • False positives from organic matter/biofilms/additives, dye uptake varies • Quantification biased by staining efficiency, bleaching, and imaging thresholds	Detecting microfibers spiked in estuarine and sea water samples	[32, 33]

View Article Online
DOI: 10.1039/D5EN01084E

The fast pace of artificial intelligence development has accelerated the integration of machine learning into both analytical detection and data interpretation in nano- and microplastic research. Across IR and Raman measurements, machine learning has improved denoising, baseline correction, feature extraction, and automated classification of polymer types, especially under low signal-to-noise or overlapping signatures [34, 35]. Recent systematic reviews highlight rapid growth in machine learning assisted analytics for nano- and microplastics in diverse water matrices, while also flagging typical failure modes such as small or biased training sets, label noise, and domain shift across instruments and matrices [34-36]. Beyond spectroscopy, machine learning enabled imaging and signal processing are beginning to support real-time, in-situ detection and quality assured quantification, pointing toward monitoring systems that connect sensors, algorithms, and models [20].

Nano- and microplastic measurement is only the beginning. Numerical models connect measurement to prediction, resolving the transport and fate of nano- and microplastic in natural waters. In aquatic systems, the fate and transport of these particles are controlled by multiscale processes such as advection-dispersion in bulk flow, Brownian-driven microscale collisions, and rapid physicochemical transformations including aging, eco-corona formation, and hetero-aggregation with natural colloids. These transformations dynamically alter effective size, density, and surface charge, shifting particle transport regimes, attachment efficiencies, and water-sediment exchange, thereby complicating modelling efforts [37-39]. For instance, eco-coronas assembled from natural organic matter, proteins, and polysaccharides can stabilize or destabilize suspensions and alter biological interactions [40]. Figure 1 provides an overview of the transformation and transport of nano- and microplastics in aquatic systems.

View Article Online
DOI: 10.1039/D5EN01084E

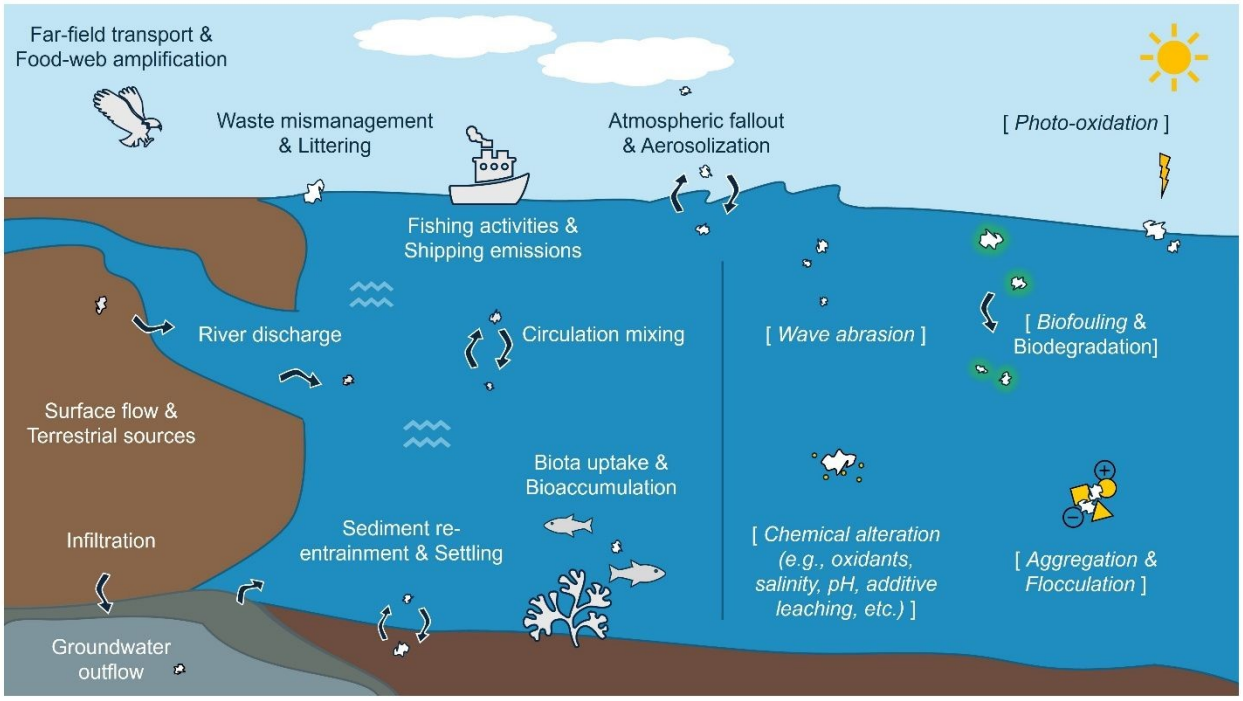

Figure 1 | Schematic overview of major transport (left) and transform (right) pathways of plastic particles in aquatic systems.

In this frontier review, we first survey recent analytical advances in detecting nanoplastic particles (Section 2), assessing detection limits, size coverage, polymer specificity, and matrix tolerance. Next, we examine how machine learning is transforming spectroscopy, imaging, and signal processing in nano- and microplastic analysis (Section 3), highlighting improvements in throughput and automation alongside persistent failure problems. We then assess microplastic fate and transport models in aquatic systems and discuss how existing model efforts can be adapted for nanoplastic particles (Section 4). Finally, we outline future directions (Section 5) aimed at developing robust, operational methods that translate particle-resolved observations into actionable guidance for monitoring, mitigation, and regulation.

2. Advances in techniques for physicochemical characterization and quantification of nanoplastics in environmental waters

Methods for detecting waterborne nanoplastics are rapidly diversifying spanning electrochemical and electroluminescent detectors, spectroscopies with active

View Article Online
DOI: 10.1039/D5EN01084E

preconcentration, label-free photonic sensors, and separation techniques coupled to mass spectrometry. Together, these approaches pursue complementary goals: polymer-specific identification, number- or mass-based quantification, and reliable operation in complex matrices. Below, we review selected recent studies organized into four themes, highlighting each method's contributions, points of convergence and divergence, and remaining gaps. Figure 2 provides a conceptual overview of this section, presenting a landscape of surveyed analytical approaches and a recommended fit-for-purpose workflow.

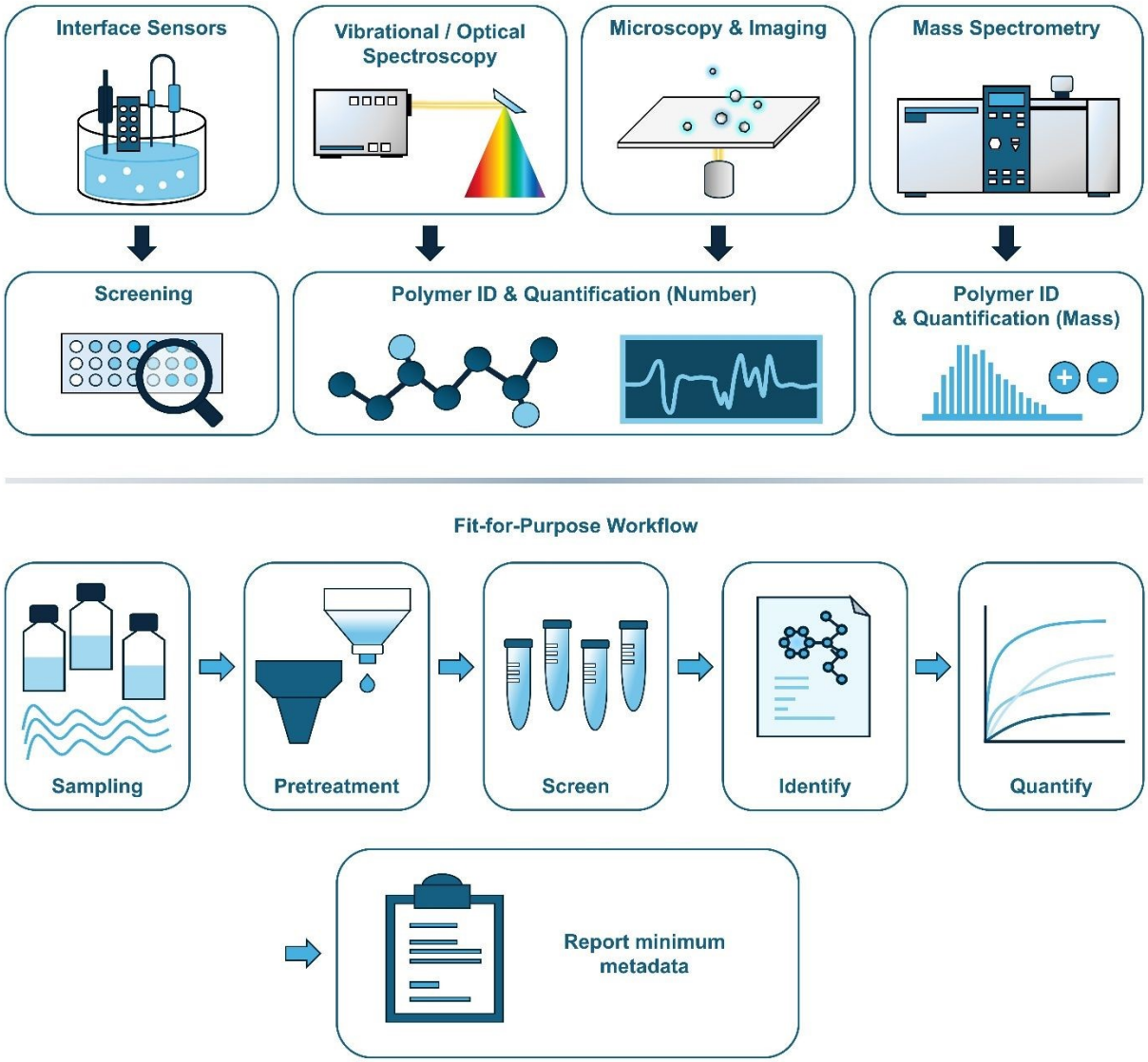

Figure 2 | Conceptual summary of Section 2, with an analytical landscape (the top panel) and a fit-for-purpose workflow (the bottom panel) for waterborne nanoplastics. The top

View Article Online
DOI: 10.1039/D5EN01084E

panel groups approaches into four classes and links each to its dominant information yield. The bottom panel outlines a recommended fit-for-purpose workflow, followed by reporting minimum metadata (e.g., particle size range, LOD/Q, matrix realism, blanks, matching criteria, recovery, and uncertainty), to support QA/QC, comparability, and reproducibility across studies.

2.1 Interface-engineered electrical and colorimetric sensors for selective nanoplastic detection

Researchers leverage interfacial chemistry, such as hydrophobicity, π-π interactions, corona dynamics, and charge, to convert nanoplastic capture into electrochemiluminescent, electrochemical, microwave, piezoelectric, or colorimetric signals.

2.1.1 Chromogenic and array-based colorimetry

These assays convert nanoplastic sorption to a chemically cross-reactive surface into a visible signal. Grumelot et al. developed a colorimetric sensor array to identify pristine, and protein-corona coated PS plastic particles (50 nm, 100 nm, and 2 μm) [41]. Five different cross-reactive chemo-responsive dyes were employed to fingerprint PS in buffered water, generating colour-difference maps and classifying patterns via hierarchical cluster analysis (HCA). Using standard chemometric analysis, the array distinguished PS from controls down to 10 ng·mL^{-1}. The platform also differentiated pristine from protein-corona coated PS at 500 – 1000 ng·mL^{-1} [41].

Complementing this, Hu et al. introduced a single-atom Fe nanozyme confined in a zeolitic imidazolate framework (ZIF) with a colorimetric assay to quantify PS nanoplastics in water [42]. In this system, PS nanoplastics adsorbed to the nanozyme through electrostatic and π-π interactions, shielding Fe active sites and suppressing peroxidase-like activity toward substrates. The particle size dependent LODs of the colorimetric sensor were 0.212 (20 nm), 4.544 (30 nm), 7.624 (50 nm), 16.955 (100 nm), and 24.171 mg·L^{-1} (150 nm). A smartphone-assisted ZIF-FeSAN visual detection platform was also examined, with LODs of 0.851, 17.564, 34.554, 67.254, and 76.124 mg·L^{-1}. In spiked tap,

View Article Online
DOI: 10.1039/D5EN01084E

lake, and drinking waters, recoveries were ~ 91.5 – 108.1% for the colorimetric sensor and ~ 90.6 – 109.0% for the smartphone platform. Selectivity tests showed a strong response to 20 nm PS but little to PE, PP, and PET, and common ions produced negligible interference [42].

Both studies exhibits significant limitations: they focused exclusively on PS, relied on buffered water rather than complex environmental matrices, and were restricted to spiked samples instead of environmental samples. These constrains limit the application of the findings to real-world conditions.

2.1.2 Charge- and mass-loading electrical detectors

Researchers use label-free devices to sense interfacial dielectric or mass changes upon particle capture. Naik et al. developed a biomimetic electrochemical impedimetric sensor for selective detection of spiked PS nanoplastics (70 nm) in tap water [43]. Drawing inspiration from mussel adhesion proteins for surface binding and electron transfer, the authors modified a carbon paste electrode (CPE) with iron-doped polydopamine (FePDA), leveraging hydrophobic π-π interactions between PS aromatic rings and FePDA for selectivity over other polymers. A lower LOD of 1 $mg \cdot L^{-1}$ was reached within a linear calibration range from 1 to 5 $mg \cdot L^{-1}$, and the recovery trails of PS spiked tap water yield 91 – 96% detection efficiency. The method's selectivity was evaluated against water-soluble, non-aromatic polymers (e.g., PEG and PVA), yet broader cross-reactivity against other common plastics and performance in complex natural matrices or with weathered particles were not reported [43].

Researchers coupled electrophoresis with a quartz crystal microbalance (QCM) to detect PE nanoplastics in water [44]. The Ti-Au QCM was operated as the anode to attract negatively charged PE, where adhesion caused resonance-frequency downshifts. A photoresist mask exposing a 1.5 mm central window concentrated deposition and enhanced sensitivity. At 10 V for 30 s per iteration, PE-spiked ultrapure water showed progressively larger shifts across repeated runs, whereas blanks remained small. The authors recommend ≤ 6 iterations to limit baseline drift from surface roughening. Applied

View Article Online
DOI: 10.1039/D5EN01084E

to waters spiked with PE, sixth-iteration shifts were larger than corresponding blanks (e.g., mineral water at 229 Hz with nanoplastics vs. 94 Hz without), and repeatability across five masked chips gave coefficients of variation of 8% in ultrapure and drinking water and 17% in mineral water. The authors indicated that the study was limited to a single polymer in spiked samples with no explicit LOD, mineral-water matrices increased mass loading, photolithographic masking was needed to gain sensitivity, and extended reuse caused baseline drift [44].

A microwave resonator approach to detect positively charged PS-NH_2 and negatively charged PS-SO_3H was proposed by Wang et al. [45]. The platform included a printed circuit board (PCB) complementary split ring resonator (CSRR) and microfabricated GaAs integrated passive device (IPD), inferring concentration from resonance frequency shifts with ~ 1.5 µL droplets. The authors synthesized PS-NH_2 and PS-SO_3H spheres in three size bins (< 50 nm, 100 – 200 nm, and > 200 nm) and measured linear responses over 0.1 – 10.0 µg·mL^{-1}. The lowest LODs were achieved with < 50 nm particles, at 9.78 ng·mL^{-1} for PS-NH_2 and 27.57 ng·mL^{-1} for PS-SO_3H. Measurements remained reliable in the presence of methyl orange dye, indicating tolerance to sample colour and some organic matter, yet demonstrations were performed in deionized water rather than environmental matrices. In addition, practical variables such as temperature or humidity drift, droplet handling, and chip cleaning can influence precision, while the higher-sensitivity IPD requires precise fabrication [45].

2.1.3 Electron-driven luminescence and photoelectrochemistry

Here, binding modulates charge transfer driven electrically or optically. Researchers presented an electrochemiluminescence assay to identify and quantify waterborne PP nanoparticles (< 220 nm), validated on leachates from disposable PP food containers and spiked tap water, with a LOD of 0.948 mg·L^{-1} [46]. The assay employed an amphiphilic perylene diimide (PDI-NH_2) probe with a persulfate coreactant, where strong probe-PP interactions yielded a selective ECL enhancement with an emission maximum at ~ 547 nm, enabling fluorescence-matched output in a standard three-electrode cell. Selectivity tests showed clear discrimination of PP, attributed to its high surface hydrophobicity,

View Article Online
DOI: 10.1039/D5EN01084E

against common plastics including PE, PS, PVC, PMMA, and PLA. The authors noted that performance was demonstrated for PP only and largely in filtered or otherwise simple matrices. The method's robustness in turbid, organic-rich environmental waters, as well as generalization across weathered particle states and broader size distributions, remained to be established [46].

A smartphone-coupled photoelectrochemical-electrochemical (PEC-EC) dual-mode sensor was built on a CdS/CeO_2 heterojunction for detecting PS nanoplastics in water [47]. The system relied on the interaction between proteins and nanoplastics, where the PS nanoparticles bound to the bovine serum albumin (BSA) surface and led to the detachment of the protein crowns from the electrodes during the aggregation process, lowering the charge-transfer resistance and enhancing the sensing signals. The sensor showed a log-linear response from 0.5 – 800 $\mu g \cdot mL^{-1}$ with LODs of 0.38 $ng \cdot mL^{-1}$ (PEC) and 9.77 $ng \cdot mL^{-1}$ (EC) for irregularly shaped PS nanoparticles (200 and 400 nm). The sensor's recoveries reached 100.37 – 103.34% in PS spiked river water, yet the demonstration was PS-specific and relied on spiked samples, broader polymer scope and native field matrices were underexplored [47].

2.1.4 Bioadhesion and active preconcentration electrochemical detection

These devices integrate biorecognition elements or mobile collectors to enhance the encounter rate prior to electrical measurement. Kim et al. introduced an epizoochory-inspired electrochemical sensor to quantify PS nanoplastics (460 nm) spiked in seawater, reaching a LOD of 0.772 $ng \cdot mL^{-1}$ [48]. In this scheme, lysozyme amyloid oligomers were drop-cast onto roughened gold electrodes, the oligomers then detached from the electrodes due to their stronger affinity with contacting nanoplastics, re-exposing the gold surface and restoring the $[Fe(CN)_6]^{3-/4-}$ redox current measured by cyclic voltammetry. The assay was evaluated across polymer types, shapes, and sizes, including irregular fragments ground from consumer PS, PE, PP, and PET re-dispersed in distilled water, and the sensor detected all four plastics while giving minimal signals for non-plastics (e.g., wood, glass, and metal). The authors noted reduced performance at the smallest sizes (e.g., 100 nm PS) and the need for matrix pretreatment to protect the sensor and mitigate

View Article Online
DOI: 10.1039/D5EN01084E

interference, indicating that universality at the nanoscale and across naturally weathered, field-collected nanoplastics requires further validation [48].

Microrobots were used to preconcentrate 50 nm carboxylated PS nanoplastics in water and then detect them using electrochemical impedance spectroscopy (EIS) [49]. The γ-Fe_2O_3/Pt/TiO_2 microrobots self-propelled under UV light and became positively charged, electrostatically capturing negatively charged carboxylated PS nanoparticles. The microrobots loaded with nanoplastics were then magnetically collected and deposited on screen printed electrodes, where the polymer layer restricted access of the $[Fe(CN)_6]^{3-/4-}$ redox couple and increased the charge transfer resistance in EIS, yielding a capture signal. The authors pointed out that the approach required ultraviolet (365 nm) illumination and operation at acidic pH around 3 to maximize capture. The evaluation was restricted to 50 nm carboxylated PS in prepared water rather than environmental samples, and a discernible EIS response was obtained only after microrobot preconcentration at particle concentrations on the order of 10^6 particles·mL^{-1}. Quantitative calibration for complex matrices was not established [49].

2.1.5 Enabling chemo(bio)sensors for dissolved plastic residues

While not particle-resolving, residue-focused sensors inform sources and co-occurring contaminants. Jebril et al. reviewed nanomaterial-enabled electrochemical chemo(bio)sensors for detecting nanoplastic residues, such as catechol, hydroquinone, bisphenol A, and resorcinol [24]. The authors surveyed methods and materials, covering voltammetric, amperometric, and impedance-based measurements with carbon, noble-metal, metal-oxide, and polymer-film modifiers, alongside enzyme, antibody, and aptamer recognition elements. Reported performance typically spans nM – μM LODs for phenolic residues, with demonstrations in tap, river, lake, dam, swamp, and mineral waters. Key limitations include matrix interferences in real waters, limited calibration standards and reference materials, biorecognition stability and electrode fouling, and the persistent gap between proof-of-concept devices and portable on-site monitoring [24].

Across interface-engineered sensors, reported LODs span from mg·L^{-1} for nanozyme systems and some impedimetric formats to ng·mL^{-1} for microwave and PEC–EC platforms.

View Article Online
DOI: 10.1039/D5EN01084E

Most demonstrations remain PS-centric owing to the wide selection of PS standards available in the market. Whereas, mostly produced PE and PP are less investigated due to their limited commercial availability and inert reactivity comparing to PS. Moreover, most research rely on spiked, relatively simple water systems only. Such patterns consistently reflected in the studies reviewed in Section 2 (Figure 3).

Apparent selectivity here in Section 2.1 typically derives from non-covalent hydrophobic and π-π interactions favouring aromatic polymers like PS, protein-corona dynamics, or surface charge. Consequently, performance often degrades for aliphatic, non-aromatic polymers such as PE and for strongly weathered plastic particles. Few studies document operational durability like fouling and baseline drift, inter-instrument reproducibility, or quantitative response functions with respect to ionic strength, pH, and dissolved organic matter. Portable units, such as smartphone-integrated PEC-EC and planar microwave and QCM devices, are promising for in-situ screening, but calibration transfer and blinded validation in real environmental waters are still needed for fit-for-purpose deployment.

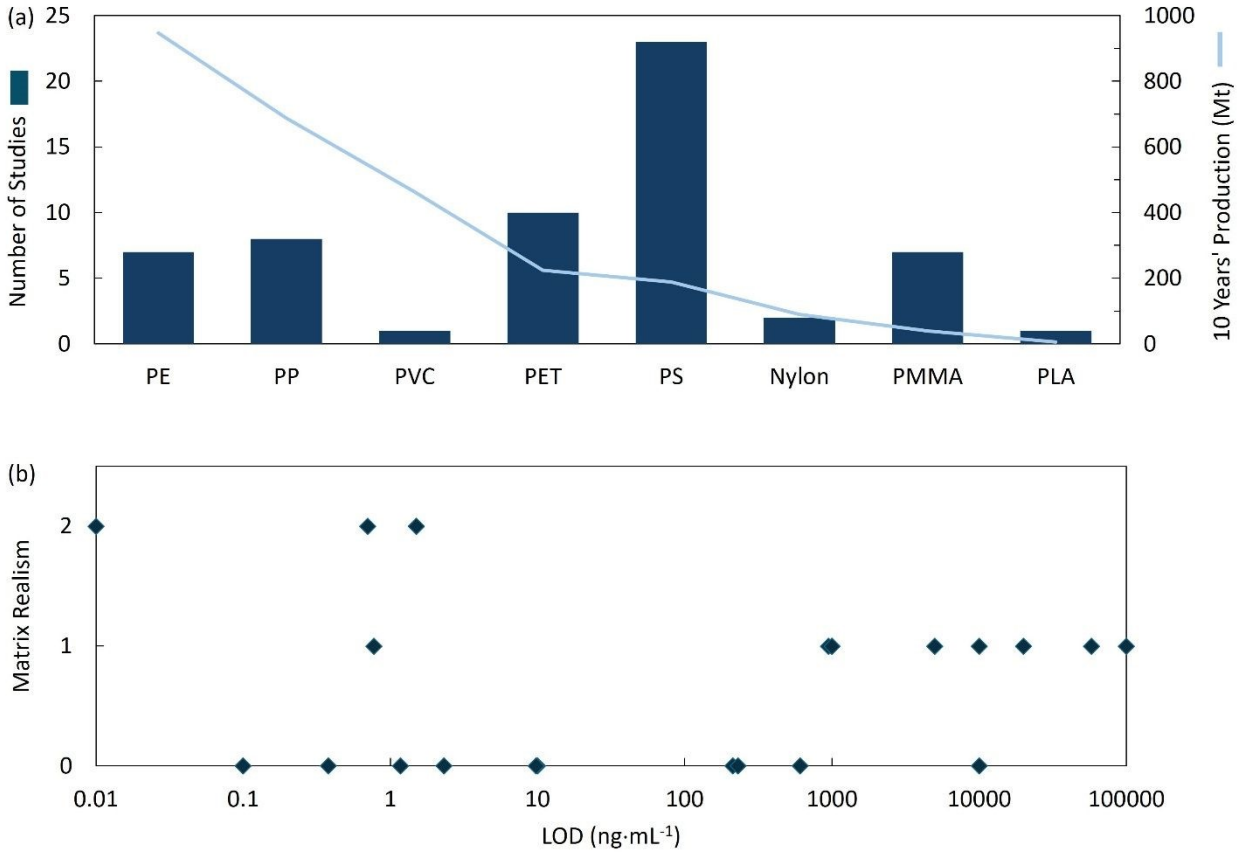

View Article Online
DOI: 10.1039/D5EN01084E

Figure 3 | (a) Polymer coverage across studies in Section 2 vs. 10 years' production estimation of the corresponding polymer. (b) Best mass LOD (ng·mL^{-1}) vs. matrix realism of studies reviewed in Section 2. Matrix realism scale: 0 = Distilled water, buffer, simulated water, or other simple laboratory matrices; 1 = Spiked real-word water samples, including environmental waters, tap water, and drinking water; 2 = Native field waters.

2.2 Raman-based and microprobe vibrational fingerprinting

Raman and microprobe vibrational techniques deliver polymer-specific fingerprints at or near the single-particle level. To overcome weak scattering and diffusion limits, recent studies combine surface-enhanced Raman spectroscopy (SERS) with active capture or interface-based enrichment, while resonance Raman and atomic force microscopy-infrared (AFM-IR) provide intrinsic chemical signatures without plasmonic amplification.

2.2.1 SERS with active or interface-based preconcentration

SERS platforms amplify weak Raman signals by concentrating particles into electromagnetic hot spots or enriching them at engineered interfaces. Recent implementations include electro-photonic tweezers, light-driven microrobots, optical tweezers paired with SERS collectors, shrinking surface-bubble deposition, self-assembled Ag-nanowire membranes, metal-phenolic aggregation, and electrochemical SERS concepts [28, 50-55]. Across these strategies, researchers aim to overcome mass transfer limits to enable polymer-specific detection and, where feasible, quantification in environmental waters.

An electro-photonic tweezers platform was used to identify 200 nm PS nanoplastics in water [50]. In this system, long-range alternating current electro-osmosis flows and dielectrophoresis (DEP) forces drove suspended nanoparticles into the Raman spot, while co-introduced gold nanorods created SERS hotspots that compensated for weak cross-sections at sub-wavelength sizes. LODs of 4.66 mg·L^{-1} and 1.17 µg·L^{-1} were reported for 200 nm and 30 nm PS nanoparticles in distilled water. The authors further demonstrated that PS and PMMA model nanoparticles exhibit distinct DEP trapping optima enabling target-specified separation, and showed operation in higher-conductivity

View Article Online
DOI: 10.1039/D5EN01084E

tap water. They noted constraints including reliance on commercially available, monodisperse spheres and simple laboratory matrices, underscoring the need for broader polymer scope, weathered particles, and native environmental waters [50].

A light-sensitive microrobot-based approach was introduced for capturing and detecting nanoplastics spiked in water [51]. The ATAR microrobots (i.e., Au/TiO_2/Au/R-Fe_3O_4) self-propelled under 400 nm light using H_2O as fuel, sweeping nanoplastics into their multilayer TiO_2/Au cages via electrostatic attraction and physical trapping. The robots were then magnetically separated, and the captured particles were analysed by SERS at the robots' Au hot spots. LODs of 1.27 μg·mL^{-1} for PS (500 nm) and 0.61 μg·mL^{-1} for PMMA (500 nm) in pure dispersions were reported. SERS confirmed recoveries of > 80% for both PS and PMMA standards spiked in river water samples. The authors noted several constraints, including reliance on monodisperse 500 nm spheres and spiked or simple matrices, scalability limited by Au cost, and the need to assess potential TiO_2 toxicity and broader biocompatibility, pointing to biodegradable alternatives and validation on weathered, low-abundance field samples [51].

An optical-manipulation and SERS platform was presented that simultaneously concentrated and quantified environmental nanoplastics in river and seawater [28]. The setup used 20 μm gold nanoparticle stacks coated with PLA as optical tweezers to drive nanoplastics under laser irradiation, and then 80 μm stacks to enrich and detect them. A brief cleaning rinse mitigated humic-acid interference that otherwise suppressed PS SERS signals, while black carbon at 10 μg·L^{-1} had negligible impact. Applied to natural waters, the platform detected PS at 6.5 – 8.5 μg·L^{-1} and PET nanoplastics at 66 μg·L^{-1} in river water, and PS at 0.7 – 1.0 μg·L^{-1} (beach) and 1.4 – 1.8 μg·L^{-1} (mariculture) in seawater. The authors noted potential eco-corona effects and recommended Fenton digestion for accurate quantitation [28].

A shrinking surface bubble deposition (SSBD) method was employed in combination with SERS for identification and scanning electron microscopy (SEM) for morphology to study nanoplastics in ocean waters [52]. In SSBD, seawater was mixed with 10 nm Ag nanoparticles, and laser heating generated a surface bubble whose Marangoni flow

View Article Online
DOI: 10.1039/D5EN01084E

concentrated suspended particles at the three-phase contact line. The co-deposited Ag nanoparticles both aided deposition and enabled SERS for chemical identification. In water samples collected across seven locations in two oceans, the authors reported nylon nanofibers, PS flakes, and PET ball-stick nanostructures. The approach is not yet quantitative, further fluid-mechanics studies are needed to relate deposited spot density to bulk concentrations [52].

Membrane filtration was coupled with SERS by self-assembling silver nanowire membranes that both preconcentrate nanoplastics and enhance their Raman signals [53]. Under controlled conditions, the membranes retained 86.7% of 50 nm standard PS particles and ~ 93.1% – 98.0% of 100 – 1000 nm PS particles. Raman mapping resolved particle distributions across 10^{-1} – 10^{-7} g·L^{-1}. The method was tested on river and seawater samples, where no nanoplastics were detected. The authors then spiked 500 nm PS standards into seawater and were able to detect them, yet the spiked river water produced no signal. The authors noted matrix effects that hindered detection in environmental waters, and the absence of a full quantitative calibration for complex matrices, despite the counting potential of Raman mapping [53].

Metal-phenolic network-mediated aggregation was combined with gold nanoparticle-based SERS and customized machine learning to enrich, identify, and quantify PS (50 nm, 500 nm, and 1 μm), PMMA (500 nm), PE (740 nm to ~ 5 μm), and PLA (250 nm) nanoplastics [54]. Applied to spiked lake water, a LOD of 10 mg·L^{-1} was reported for all four types of plastics, with classification accuracies > 95% for PE, PS, and PMMA, and ~ 74% for PLA. Recoveries in spiked matrices were ~ 80 – 120% for PS and PMMA, while PLA at low concentrations and PE in lake water showed lower recoveries, reflecting matrix interferences (e.g., metal-ion competition with Zr^{4+} for tannic acid) and weaker PE Raman band at 1297 cm^{-1}. Limitations noted by the authors include higher LODs in complex waters, challenges in PLA identification at low concentrations due to potential biodegradation, the need to re-establish PE calibration in lake water, and evaluation constrained by the limited set of commercially available nanoplastic types and sizes [54].

View Article Online
DOI: 10.1039/D5EN01084E

A perspective was presented by Yang et al. on coupling electrochemistry with SERS as a dual-mode nanoplastic sensing system, leveraging electrochemistry's quantitative capability together with SERS's polymer-specific fingerprints [55]. The authors highlighted potential-controlled electrosorption to preconcentrate nanoplastic particles at SERS hot spots, and electrochemical deposition and activation to build and refresh hot-spot-rich conductive substrates. They also described SERS-assisted electrochemical workflows that identify polymer type and profile surface adsorbates, while the electrochemical channel provides concentration and kinetic information [55].

SERS methods succeed by concentrating analytes, but the same capture physics can bias results by size, charge, and shape, while organic matter and salts in the water can reduce the signal. Robust use therefore requires reporting and correcting for preconcentration factors, capture efficiencies, and recoveries, along with strategies to refresh hot spots and mitigate fouling.

2.2.2 Resonance Raman and AFM-IR fingerprinting

Here we review selected intrinsic fingerprinting methods that do not rely on plasmonic enhancement. Cârdan et al. revealed that the copper-phthalocyanine blue pigment (PB15) embedded in aged blue plastics produced a strong resonance-Raman signal that enabled confocal micro-Raman detection of environmentally derived blue nanoplastics down to ~ 500 – 800 nm, even when polymer bands were absent. Surveying naturally weathered plastics including LDPE, HDPE, PP, PS, and PET, PB15 occurred in 81% of blue/green macroplastics and 51% of blue microplastics. The authors also noted potential spectral interferences from plant- and animal-derived, blue-dyed fibres but highlighted their distinct coloration chemistry and Raman profiles. The study framed PB15 as a double-edged marker, i.e., a Trojan-horse risk coupling pigment and plastic, and an opportunity to target blue nanoplastics in complex environmental matrices [56].

Dielectrophoresis was combined with Raman spectroscopy to trap and identify nanoplastic particles in suspension [57]. The electric field generated negative dielectrophoresis, concentrating particles into the Raman confocal volume for 30 s before acquisition. In bottled drinking water spiked separately with each polymer, 200 nm PS,

View Article Online
DOI: 10.1039/D5EN01084E

180 nm PP, and 100 nm PET were identified at ~ 20 μg·mL^{-1}. The authors indicated that direct injection into the dielectrophoresis cell minimizes interference from dissolved salts, but more complex matrices like tap or environmental water will require pretreatment such as cascade filtration, enzymatic or chemical digestion, and preconcentration [57].

AFM-IR was used to identify nanoplastics in surface seawater (0.1 – 1.0 m depth) [14]. After sequential filtration and ethanol-assisted deposition to suppress coffee-ring effects, particles were screened by optical microscopy and SEM and energy dispersive X-ray (EDX), then chemically assigned by AFM-IR. The authors identified nanoplastics including highly crystalline poly(3-hydroxybutyrate) (~ 700 nm) and a bisphenol-A based epoxy (~ 860 nm), alongside polyester microplastics. They also noted the method's low throughput and the value of pairing it with mass spectrometry methods to provide quantitative context [14].

2.2.3 Plasmonic binding sensors without Raman enhancement

A nano-plasmonic biosensor was developed to detect and quantify nanoplastic particles in seawater [58]. PMMA (100 nm) was used as a nanoplastic model for control tests. The platform grafted estrogen receptor onto a polymer-based gold nanograting (ER-GNG) so that ER-PMMA binding modulated hybrid surface plasmon resonance (SPR) and localized surface plasmon resonance (LSPR), display as a characteristic blue-shift in the plasmonic resonance. The method was applied to real seawater, where 1.5 ng·mL^{-1} in the 1:20 dilution of nanoplastics was detected without further sample pretreatment, while the polymer type was unspecified [58].

Across the methods surveyed, SERS platforms offer the highest sensitivity but require careful control of capture bias, hot-spot stability, and matrix effects. Resonance Raman and AFM-IR provide chemical assignments at lower throughput. Plasmonic binding sensors enable simple, label-free monitoring but lack spectral identification. Priority next steps are to adopt matrix-matched calibrations, develop certified reference materials, routinely report preconcentration factors, capture efficiencies, and recoveries, conduct blinded tests on environmental waters, and evaluate performance with weathered plastics.

View Article Online
DOI: 10.1039/D5EN01084E

2.3 Label-free photonic and refractometric sensors for number-focused quantification

Label-free photonic and refractometric platforms quantify nanoplastic particles by converting changes in light scattering, optical interference, laser-induced breakdown, or fluorescence lifetime into concentration measurements.

A laser-backscattered fibre-embedded optofluidic chip (LFOC) was developed to quantify nanoplastics spiked in water [59]. In the device, a 635 nm beam was launched and collected through a single-multimode fibre coupler, and the 180° back-scattered signal scaled linearly with both mass concentration and particle number. Across 20 – 500 nm PS, LODs were 60.00, 19.75, 1.22, 0.23, and 0.39 $\mu g \cdot mL^{-1}$, respectively. The quantitative approach also extended to 200 nm PE, PET, PMMA, and PP using a universal calibration with a LOD of 1.08 $\mu g \cdot mL^{-1}$. Spiked river water samples yield 95.56 – 114.47% recoveries. The authors noted several limitations: the platform did not provide polymer-specific chemical identification; performance depended on particle size and optical conditions (e.g., refractive-index effects on Fresnel reflections); number concentrations were inferred from size and density rather than directly counted; and real-world evaluation relied on spike-and-recovery rather than native field or weathered particles [59].

Laser-induced breakdown detection (LIBD) was evaluated as a particle counting approach for nanoplastics in water [60]. In LIBD, a focused laser irradiated the suspension, then multiphoton ionization produced seed electrons that absorbed energy via inverse Bremsstrahlung and avalanched to a dense plasma, launching a shockwave recorded as optical plumes or acoustic spikes. Irregular, polydisperse PS, PP, and PET nanoplastics (~ 100 nm) generated from single-use plastic products and dispersed in a simple saline electrolyte yielded LODs of 1×10^4 – 3×10^5 particles$\cdot mL^{-1}$. Sensitivity depended on particle size, concentration, and material properties (i.e., density, ionization energy, optical attenuation, and aggregation), generally favouring hard over soft particles. The authors noted that water chemistry and multimodal size distributions could shift breakdown probability and mask smaller particles, and they recommended coupling LIBD

View Article Online
DOI: 10.1039/D5EN01084E

with size-separation approaches and exercising caution when extrapolating from PS-based calibrations [60].

A fluorescence lifetime analysis (FLA) system was presented that uses label-free fluorescence with fit-free phasor analysis of time-correlated single-photon counting to detect model PS nanoplastics in water [61]. The method detected unmodified PS suspensions with a LOD of 0.01 $mg \cdot mL^{-1}$. Validation used commercial PS models, including PS-nano (121 nm) and PS-micro (1.35 μm), with fluorescent COOH-PS (35.8 nm) and NH_2-PS (140 nm) as references. Phasor modulation scaled with concentration, enabling calibration-style quantification, while the phase lifetime remained characteristic of the particle type. The authors noted current constraints where evaluation limited to PS in water and polymer differentiation not yet demonstrated, highlighting the need to lower the LOD further and to distinguish among plastics in more complex matrices [61].

An optical microfiber Mach-Zehnder (M-Z) interferometer sensor was proposed by Li et al. for detecting PS nanoparticles (100 and 150 nm) in water [62]. A tapered microfiber supported two-mode interference, and adsorption-induced refractive-index changes in the evanescent field shifted the transmission spectrum. An aminated surface decorated with L-phenylalanine (L-PHA) captured PS via π-π stacking for selective monitoring. In simulated environmental water samples, LODs were 2.31×10^{-6} $mg \cdot mL^{-1}$ and 2.96×10^{-6} $mg \cdot mL^{-1}$ for 150 nm and 100 nm PS, respectively. The authors reported measurable wavelength shifts in nine PS spiked environmental waters including lakes, seawater, and wastewater, without providing recoveries or other quantitative results [62].

In a model simulation study, a plasmonic refractive index sensor for potential nanoplastic detection in water was proposed by Guchhait et al. [63]. The device comprised a metal-insulator-metal (i.e., Ag-air-Ag) waveguide side-coupled to a concentric square-ring resonator and was simulated in 2D using COMSOL finite-element optics. Surface plasmon modes in the waveguide produced transmission resonances that shifted with the local refractive index (n) inside the resonator as the sample filled it. In an initial nanoplastics scenario with $n_{water} \approx 1.34$ and $n_{nanoplastics} \approx 1.5$, the system exhibited a linear resonance shift for $\Delta n = 0.00025 – 0.001$, corresponding to 0.15625 – 0.625% plastics in

View Article Online
DOI: 10.1039/D5EN01084E

water (v/v). The authors cautioned that temperature, salinity, and co-present particulates can also shift refractive index, and suggested adding a plastic-binding peptide to enhance specificity [63].

Label-free photonic sensors provide rapid, compact measurements with competitive LODs, but their signals are generally not specific to polymer type and are sensitive to matrix factors such as refractive index, salinity, and dissolved organic matter. Calibrations can misestimate concentrations when particle sizes or shapes vary, and number concentration is often inferred rather than directly counted unless sizing is built in. In practice, these platforms can be potentially used as front-end screens or counters that access samples for follow-up, chemically specific confirmation.

2.4 Separation-based workflows and mass spectrometry routes for chemically resolved quantification

Separation-centric approaches decouple particle size, composition, and matrix effects, enabling polymer identity and abundance to be quantified with reduced ambiguity. Coupling these separations to mass spectrometry provides a bridge between particle-number measurements and polymer-specific mass detection.

Capillary electrophoresis with an ultraviolet-visible (UV-vis) spectrophotometric diode-array detector (DAD) was developed for size separation and detection of PS and PMMA nanoplastic spheres under alkaline conditions [64]. Experiments were run at pH 8.9 for PS (30 – 300 nm) and at pH 11.9 for PMMA (50 – 200 nm), with LODs on the order of 10^{11} particles·mL^{-1} for PS and ~ 5 × 10^{11} particles·mL^{-1} for PMMA. The study also quantified nonlinear electrophoresis at high fields and reported size-dependent effective mobility, with surface charge density decreasing as size increased. Demonstrations were limited to buffered suspensions, while no environmental waters were tested. Limitations noted by the authors also include low sensitivity for real samples, potential capillary clogging or tailing above ~ 300 nm, UV interferences and peak overlap for mixtures, and a need for preconcentration. The authors further suggested downstream MS coupling for a more comprehensive analysis [64].

View Article Online
DOI: 10.1039/D5EN01084E

A pyrolysis-gas chromatography mass spectrometry (Py-GC-MS) workflow was developed for nanoplastic particles and agglomerates (10 – 1000 nm) in environmental waters [65]. Following H_2O_2 oxidative cleanup, samples were firstly passed through a 1 µm filter and then concentrated with a 100 kDa stirred-cell ultrafiltration step prior to pyrolysis. Polymer identification and quantification relied on selected indicator ions, for example, styrene dimer and trimer for PS, C_{18} – C_{21} n-alkadienes for PE, and vinyl-benzoate species for PET. The authors reported < LOD – 0.76 µg·L^{-1} PE, 0.18 – 0.25 µg·L^{-1} PET, 0.32 – 0.51 µg·L^{-1} PS, < LOD – 0.59 µg·L^{-1} PP, and < LOD – 0.04 µg·L^{-1} Nylon 66 nanoplastics in surface water, reservoir water, and stormwater [65].

Li et al. combined asymmetric flow field-flow fractionation (AF4) coupled with multi-angle light scattering (MALS) and Py-GC-MS to obtain size-resolved particle counts and polymer-specific mass quantification of nanoplastics in water [66]. AF4-MALS provided calibrated models to infer concentration and particle number from MALS peak area and size, while Py-GC-MS identified PS and PMMA via styrene and methyl methacrylate pyrolysates and quantified mass. For PS (60 – 300 nm) without preconcentration, AF4-MALS showed size-dependent LODs of 0.5 – 5 ppm. Py-GC-MS quantification used indicator ions with linear calibrations for styrene (0.02 – 8 µg, PS) and methyl methacrylate (0.03 – 10 µg, PMMA), and an estimated LOD of 0.01 µg for both markers. In bottled water spiked with 200 nm PS and 100 nm PMMA, Py-GC-MS confirmed polymer identity and yielded mass-based overall recoveries of 81.5% (PS) and 69.4% (PMMA), complementing AF4-derived fractional recoveries of 57.2 – 61.0%. The authors further noted that preconcentration is essential yet risks pore clogging and morphology change, which can depress AF4 recovery and underestimate concentrations [66].

Nanoplastics were identified and quantified across the North Atlantic using thermal-desorption proton-transfer-reaction mass spectrometry (TD-PTR-MS) [19]. Along a transect from the subtropical gyre to the European shelf, the authors measured ~ 1.5 – 32.0 mg·m^{-3} of PET, PS, and PVC throughout the water column. They reported mixed-layer (10 m below sea level) totals were ~ 1.4 times higher than at intermediate depth, with the highest values near Europe. Intermediate depth (1000 m below sea level) totals were ~ 1.8 times higher inside the gyre. Bottom waters (30 m above the seafloor offshore

View Article Online
DOI: 10.1039/D5EN01084E

and 5 – 10 m above the seafloor at coastal sites) averaged ~ 5.5 $mg \cdot m^{-3}$ and dominated by PET. The mixed layer of the temperate-subtropical North Atlantic was extrapolated to ~ 27 million tonnes. The authors note that reported concentrations were lower limit estimates because thermal desorption and ionization convert only part of the plastic into detectable ions. Spike-and-recovery tests for PS gave about ~ 7% recovery, indicating that true PS levels may be higher. Monte Carlo simulations showed that any overestimation driven by organic matter would fail before exceeding ~ 31%. PE and PP were not detected, which the authors attributed to possible chemical alteration in seawater, masking by organic matter, or concentrations below LOD. The one micrometre prefilter also removed most marine snow, so larger aggregates were excluded [19].

Mass spectrometry approaches provide polymer-specific mass measurements and are generally less affected by additive composition, but they often trade throughput for selectivity and sample preparation steps can alter particles. AF4 links particle sizing with mass quantification, yet results depend strongly on membrane chemistry and on how the sample was collected, stored, and pretreated. Py-GC-MS studies have shown that false positives and associated overestimation can arise in complex, organic-rich matrices because endogenous constituents, notably lipids, can generate nonspecific pyrolysis products that overlap with polymer marker profiles, particularly for PE and PVC [67, 68]. Accordingly, Py-GC-MS quantification in biotic or lipid-rich environmental samples should be supported by strict cleanup, procedural blanks/controls, careful marker selection, and orthogonal confirmation to minimize misassignment and overreporting. Environmental samples analysed by TD-PTR-MS in the lab have yielded polymer-related ion signals, though recoveries are often low and some polymers are missed, underscoring the need for certified reference materials, inter-laboratory harmonization, and careful spike-recovery evaluation in real matrices.

Across nano- and microplastic research, translating quantification between particle number-based metrics (e.g., FTIR and Raman particle counting) and mass-based metrics (e.g., thermal and MS approaches) remains a challenge. Conversions require assumptions about particle size distributions, morphology (e.g., fibres vs fragments), and polymer density, yet these parameters are often incompletely reported and can vary

View Article Online
DOI: 10.1039/D5EN01084E

substantially across matrices and weathering states. Method-specific detection windows further bias which size fractions are captured, making back-calculation non-unique and limiting direct comparability across studies that quantify on different bases [69, 70]. Recent reporting and standardization efforts therefore emphasize transparent documentation of size bins, shape classes, and quantification basis to enable more defensible inter-study comparisons and, where attempted, conversions.

3. The incorporation of machine learning with analytical approaches

The rapid advancement of machine learning has opened new opportunities for detecting nano- and microplastics in aquatic systems. Conventional spectroscopic, spectrometric, and imaging-based techniques are often limited by labour-intensive workflows, operator bias, and the inherent difficulty of distinguishing plastics from natural colloids and other nanoscale or microscale particles [34, 71, 72]. By applying data-driven algorithms, machine learning offers a path to improved signal processing, extraction of meaningful patterns from complex datasets, and automated classification [34, 71-73]. These capabilities hold promise for streamlining workflows and achieving more consistent results, while accelerating the transition of laboratory techniques into scalable, field-deployable monitoring systems. In what follows, we organize recent progresses before analysing cross-cutting needs and outlook. Figure 4 summarizes how machine learning methods are integrated across diverse analytical techniques for nano- and microplastic analysis, while highlighting the key challenges that constrain robust performance across matrices, size regimes, and deployment contexts.

View Article Online
DOI: 10.1039/D5EN01084E

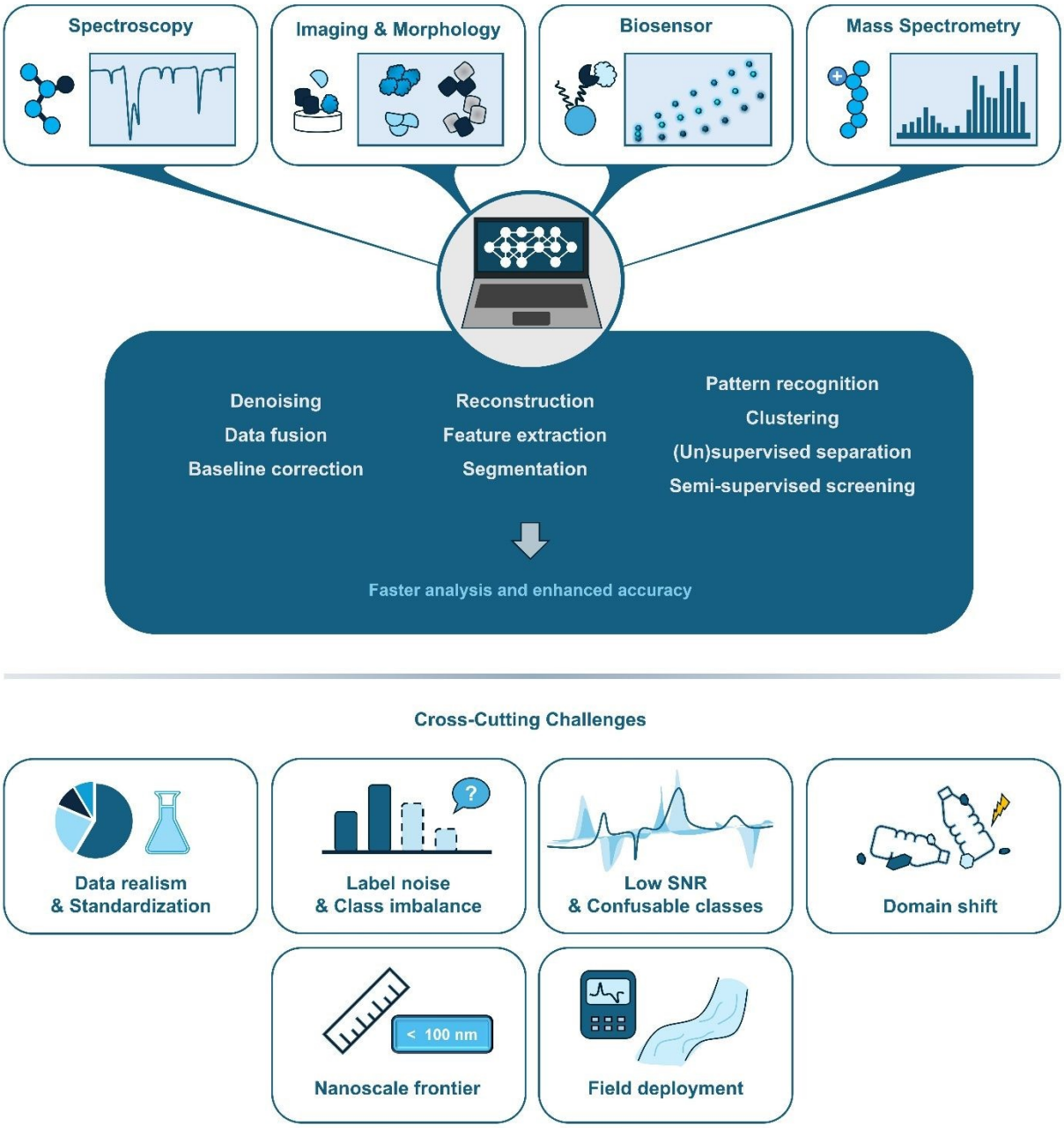

Figure 4 | Machine learning enabled integration of analytical modalities for nano- and microplastic analysis and associated cross-cutting challenges. Top panels illustrate representative analytical inputs feeding into machine learning workflows. Central processing steps collectively enable faster analysis and improved classification accuracy. Bottom panels summarize cross-cutting challenges that limit robust deployment across matrices and scales.

View Article Online
DOI: 10.1039/D5EN01084E

3.1 Spectroscopy-based detection

Spectroscopy provides chemically specific fingerprints. Machine learning is predominantly leveraged in this field for denoising, reconstruction, feature extraction, and classification under low signal-to-noise.

3.1.1 Infrared spectroscopy

A machine learning-based workflow for polymer identification from Fourier transform infrared (FTIR) spectra of microplastics was proposed by Liu et al. [74]. To address baseline shifts, noise, and interfering peaks that often compromise FTIR analysis, the authors employed two deep learning reconstruction models, including an autoencoder (AE) and a V-like convolutional neural network (VCNN), to enhance spectral quality prior to classification. Four classification models were trained, including decision trees, random forest, linear support vector machines, and one-dimensional convolutional neural networks, for microplastic identification. The workflow retained practical value with a top-1 accuracy of 71.43% and top-3 accuracy above 90% when applied to environmental datasets, while the authors noted that the approach was limited by an inadequate and biased environmental dataset, augmentation methods that did not capture real-world weathering and oxidation, and the potential for deep learning-based reconstruction to introduce additional noise and spectral distortions [74].

A dense feed-forward neural network (DNN) was assessed for automated classification of FTIR spectra of environmental microplastics, benchmarking its performance against other machine learning models and human annotations [75]. Trained on an aggregated dataset spanning 16 polymer categories from diverse marine and freshwater sources, the DNN delivered higher precision and F1 scores than alternative approaches. The model also revealed systematic mislabelling in public FTIR datasets and correctly re-assigned spectra that human annotators had misclassified [75].

A deep learning-assisted spectroscopy fusion framework was introduced for the identification of microplastics using Raman and attenuated total reflection Fourier transform infrared (ATR-FTIR) spectra [76]. A one-dimensional convolutional neural

View Article Online
DOI: 10.1039/D5EN01084E

network (1D-CNN) with an embedded multi-head attention mechanism was trained on eight polymer types, reaching 73% and 75% accuracy with ATR-FTIR and Raman spectra, respectively. The authors also proposed a three-level fusion strategy that combined complementary information from ATR-FTIR and Raman to enhance the recognition performance. The model yielded progressively higher accuracies with increased level of fusion data, and was validated in detecting PMMA microplastics spiked in tap water [76].

Tian et al. paired quantum cascade laser-based IR (LDIR) with a hybrid machine learning workflow to identify weathered microplastics in surface and drinking water. The authors trained ensemble supervised classifiers, i.e., subspace k-nearest neighbour (Sub-kNN) and boosted decision tree (BDT), on spectrum characteristics of a labelled subset and applied confidence thresholds to scale predictions to the full dataset. Low confidence spectra were then clustered with a density-based spatial clustering of applications with noise (DBSCAN) model guided by a t-distributed stochastic neighbour embedding model, followed by domain experts labelling efforts. The authors noted that the methodology can be constrained by the availability of quality labelled spectra for training, and that classification is bounded by the set of predefined categories, with other polymers treated as outliers. They also noted that the heterogeneous non-plastic fraction can be difficult to group cleanly and may be falsely labelled as plastic, and that DBSCAN outcomes depend on pragmatic, subjective choices of parameters (e.g., the minimum number of points and the neighbourhood searching radius) that affect the balance between clusters and outliers [77].

3.1.2 Raman spectroscopy

An automatic workflow for the identification of PS and PVC nanoplastics in rainwater was implemented by combining highly reflective aluminium substrates with Raman spectroscopy and machine learning [78]. To overcome weak Raman signals and noise interference typical of nanoscale particles, the authors applied a peak extraction and retention (PEER) algorithm for spectral pre-processing, followed by training a random forest model comprising 100 uncorrelated decision trees. The model was developed on

View Article Online
DOI: 10.1039/D5EN01084E

five polymers, including PE, PTFE, PS, PMMA, and PVC, and reached an average classification accuracy of 98.8%, despite the inherent difficulty of separating PE from PTFE and PMMA from PVC because of overlapping spectral features. Compared with support vector machine (SVM) and back propagation (BP) neural networks, the random forest outperformed both, particularly in handling low signal-to-noise spectra [78].

Qian et al. introduced a hyperspectral stimulated Raman scattering (SRS) microscopy platform integrated with a data-driven spectral matching algorithm to achieve single-particle chemical imaging of nanoplastics [15]. By employing a narrowband SRS imaging scheme, the system reached LODs down to below 100 nm, while the tailored algorithm enabled polymer identification across seven common plastics, including polyamide (PA), PP, PE, PMMA, PVC, PS, and PET. Beyond quantification, multidimensional profiling of particle size, morphology, and composition uncovered noticeable heterogeneity and nonorthogonality between different plastics. The authors applied the method to bottled water as a model system and reported average concentrations of $2.4 \pm 1.3 \times 10^5$ nano- and microplastic particles per litre [15].

An agarose-based microfiltration device was paired with Raman spectroscopy and a convolutional neural network (CNN) to identify 100 nm PS nanoplastics in deionized water and filtered seawater [79]. Raman spectra were pre-processed and augmented before being analysed with a fine-tuned CNN focused on the polymer fingerprint region. The approach achieved a LOD of 6.25 $\mu g \cdot mL^{-1}$ while reducing mapping time by 50%. The CNN also outperformed true component analysis (TCA) under shortened acquisition times (i.e., 0.2 and 0.1 s per point), maintaining ≥75% prediction confidence, whereas TCA failed due to low signal-to-noise ratios. Occasional false positives occurred under weak signal intensities, pointing to the need for further noise-reduction and signal-enhancement strategies [79].

3.1.3 Fluorescence labelling and imaging

Image-based quantification of microplastics in bottled water was advanced by introducing an Ilastik-trained random forest classifier for semantic segmentation of Nile Red-stained fluorescence microscopy images [80]. The classifier was trained on images of blanks,

View Article Online
DOI: 10.1039/D5EN01084E

bottled water samples, and stained microplastic standards including PE, polyamide-6 (PA 6), PET, and polyvinylidene chloride (PVDC). This supervised learning workflow replaced conventional thresholding approaches by generating binarized masks, which were then refined in ImageJ using watershed and noise-reduction functions. The method demonstrated a minimum detectable particle size of 10 μm, with particle count detection and quantification limits of 28 and 85 particles per 500 mL, respectively. When applied to 20 bottled water samples, the method reported microplastic abundances ranging from below detection to 7237 items per 500 mL [80].

Extending this concept, Meyers et al. evaluated decision tree and random forest algorithms for automated Nile Red-based identification of pristine microplastics, and plastic particles weathered under semi-controlled marine environments [81]. Five types of uncoloured microplastics with heterogeneous shapes, including PE, PET, PP, PS, and PVC, were deployed for 12 months in subsurface coastal waters and at deep-sea sites to undergo natural weathering. Both models reported > 90% accuracy for detecting and identifying pristine particles, while random forest classifiers outperformed decision tree models in identifying weathered plastics. A lower LOD of 2 – 4 μm was reached [81].

A laser-induced fluorescence (LIF) system was coupled with machine learning algorithms for the identification of predominantly uncoloured, known microplastics in simulated marine water [82]. Using 405 nm laser excitation, fluorescence spectra of plastics, including PE, PP, PS, and PET, together with common marine materials, were recorded and pre-processed with principal component analysis before classification. A two-step machine learning workflow first distinguished plastics from non-plastic organics with 97.6% accuracy and then identified polymer types with 88.3% accuracy. The authors noted challenges such as spectral overlaps from pigments or biofilms, which may obscure plastic signals, and emphasized the need for further validation with more diverse and coloured samples [82].

A wireless portable device was engineered for quantifying nano- and microplastics by integrating machine learning algorithms with fluorescence imaging [83]. PS nanoparticles (50 nm) spiked into tap water were labelled and concentrated using a luminescent metal

View Article Online
DOI: 10.1039/D5EN01084E

phenolic networks (L-MPNs) supramolecular labelling strategy for fluorescence-based detection. A customized MATLAB code executed on a smartphone converted raw fluorescence microscopic images into quantitative outputs, while a decision tree model embedded in the system facilitated the analysis across diverse particle sizes and concentrations. The lower boundaries of the size-dependent LODs ranged from 330 particles for 10 μm microplastics to 2.58 × 10^8 particles for 50 nm nanoplastics under optimized labelling conditions [83].

3.2 Imaging and morphological analysis

Unlike spectroscopy, morphology-centric pipelines classify particles using shape, phase, and dynamical features, even when polymer chemistry is not explicitly available, offering label-free throughput but requiring careful validation against chemical identities.

3.2.1 Optical and light-based imaging

Photoacoustic imaging-assisted deep learning was used to characterize microplastics sourced from environmental water samples [84]. After laboratory screening and FTIR confirmation, six representative morphologies, including flakes of PVC, granules of PP, loops of PVC, ovals of PVC, rods of PP, and fragments of PE were selected, alongside non-plastic controls. To address limited datasets, the authors developed an automated pre-processing pipeline using the Segment Anything Model (SAM), thresholding, and contour-based anchor box slicing to generate segmentation masks and extract individual sample images, thereby expanding the dataset without extensive manual labelling. These data were then used to train a generative deep learning model with dual proxy tasks, which enabled unsupervised segmentation, target detection, and classification of microplastic morphologies independent of polymer type [84].

A lensless shadow microscopy (LSM) strategy combined with deep learning-based object detection algorithms (i.e., You Only Look Once (YOLO)) was introduced for quantifying abraded sponge microplastic fibres spiked into natural waters [85]. The custom LSM system offered a field-of-view > 1 cm^2 with submicron-pixel resolution (~ 500 $nm \cdot pixel^{-1}$), while the algorithms automatically classified and measured linear and branched fibres in

View Article Online
DOI: 10.1039/D5EN01084E

projection images. The method reported a LOD of 10 items·mL^{-1} and was validated across dispersed and aggregated fibres as well as natural water matrices. The authors noted that sample transfer losses and the lack of chemical characterization remain limitations, highlighting the need for complementary spectroscopic methods and optimized handling procedures [85].

A machine learning-integrated droplet microfluidic system, named MiDREAM, was presented for the quantification and size classification of spiked PS microspheres in water [86]. The system encapsulated microplastics into uniform droplets (~ 142 µm diameter) and combined phase-contrast imaging with an optimized You Only Look Once (YOLO) v8 convolutional neural network for automated detection. The method differentiated PS microspheres across size classes from 3 to 50 µm and outperformed hemocytometer counting and surface enhanced Raman spectroscopy (SERS) in accuracy. The approach was demonstrated using spiked PS particles in environmental water matrices, while distinguishing plastics from non-plastic particulates in real-world samples requires complementary chemical confirmation [86].

An artificial intelligence-assisted nano-digital inline holographic microscopy platform was introduced for the automated characterization and classification of nano- and microplastics in natural waters [20]. From raw holograms, over 20 morphological parameters, including particle size, shape, perimeter, optical phase, surface roughness, area, and edge gradient, were extracted to train deep neural network classifiers under supervised learning. The system reached characterization and classification rates of 1.4 and 25 particles·s^{-1}, respectively, and identified ~2% and ~1% of suspended particles as plastics in lake and river waters. The authors applied size correction approaches to address the overestimation observed at the nanoscale and further highlighted the need for optimized setups and improved numerical reconstructions to extend the LOD below 100 nm [20].

3.2.2 Electron microscopy-based imaging

Researchers sought to couple scanning electron microscopy (SEM) with a UNet-based computer vision algorithm to differentiate plastic particles (~1 µm) from other materials by

View Article Online
DOI: 10.1039/D5EN01084E

tracking spatiotemporal deformation behaviour under electron beam irradiation [87]. Lower-crystallinity polymers such as PVC and PET exhibited distinct shrinkage patterns compared to HDPE and non-plastic media, and blinded sample tests confirmed the approach could identify plastics within laboratory-prepared mixed matrices. The authors noted that the integration of deep learning enabled automated segmentation and deformation analysis, reducing reliance on manual measurements, while constraints remained, including variability from particle size and shape, deviations between manual and computational results, and noise in the automated dataset [87].

3.3 Biosensor platforms

Beyond optical contrast, receptor-based sensors encode binding kinetics and selectivity in electrical and optical transduction signals that machine learning can disentangle across particle size and chemistry.

Researchers developed a peptide sensor-based strategy combined with machine learning for the identification of acrylate- and methacrylate-type polymeric nanoparticles in water [88]. Short peptides conjugated with a microenvironment-sensitive fluorophore produced distinct fluorescence spectra upon interacting with nanoparticles of different polymeric compositions. Both supervised (i.e., linear discriminant analysis) and unsupervised (i.e., principal component and hierarchical cluster analyses) machine learning algorithms were applied to these signal patterns, enabling discrimination between homopolymeric and copolymeric nanoparticles. The authors noted that while the method could differentiate nanoparticles with slightly different chemical structures, the study was conducted on as-synthesized polymeric nanoparticles with controlled sizes and compositions, which may not fully capture the heterogeneity and weathering of environmental nanoplastics, and that the relatively simple linear algorithms employed may face limitations when applied to more complex or noisy datasets [88].

A proof-of-concept sensor was presented for the selective identification of PS and PMMA particles at both the nanoscale (100 nm) and microscale (20 μm) by coupling a plasmonic probe with supervised machine learning [89]. The sensor was based on an ER-SPR-POF platform, in which estrogen receptors (ER) were immobilized on a gold-coated plastic

View Article Online
DOI: 10.1039/D5EN01084E

optical fibre (POF) to induce a surface plasmon resonance (SPR) response. Shifts in the plasmonic resonance wavelength, arising from binding interactions between plastic particles and the receptor, were analysed as input features for a predictive machine learning model built with MATLAB's Statistics and Machine Learning toolbox. This approach enabled classification of both polymer type and particle size. To demonstrate environmental applicability, the system was further tested in simulated seawater spiked with PMMA nanoplastics [89].

3.4 Mass spectrometry

Mass spectrometry converts particles to diagnostic fragments and time-profiles, where machine learning organizes these high-dimensional signatures for class discovery and screening.

Researchers showcased fast chemical screening of plastic particles ranging from 500 nm to 20 μm in aerodynamic diameter by combining chromatography-free thermal desorption and pyrolysis mass spectrometry with unsupervised and semi-supervised machine learning [90]. After acquiring polymer-specific fingerprints and time-resolved release profiles, the authors first applied principal component analysis (PCA) for data reduction and projected the spectra onto the resulting components. They then employed Gaussian mixture models (GMM) and fuzzy *c*-means (FCM) clustering to differentiate, cluster, and interpret the mass spectral data. The study was conducted on controlled nano- and microplastic suspensions generated in the laboratory, without direct extension to environmental samples [90].

3.5 Cross-cutting themes, limitations, and outlook

Machine learning is improving consistency and throughput across spectroscopy, imaging, biosensing, and mass spectrometry, but several shared bottlenecks determine real-world performance. Synthesizing insights from selected studies together with recent reviews, we discuss existing challenges and propose a forward-looking agenda grounded in demonstrated practice.

3.5.1 Data realism, standardization, and model robustness

View Article Online
DOI: 10.1039/D5EN01084E

Dominant sources of error in machine learning-assisted analytical workflows are data scarcity, label noise, and domain shift. Models are sometimes trained on small, biased datasets with inconsistent annotations, then face shifts between pristine and weathered particles and between laboratory and environmental matrices (Figure 5). For instance, Liu et al. noted biased environmental spectra and unrealistic augmentations for FTIR [74]; Herb et al. uncovered systematic mislabels in public FTIR data sets [75]; Meyers et al. documented performance drops on weathered versus pristine particles [81]; Gong et al. reported false positives at low signal-to-noise ratios in Raman mapping [79]. Researchers urge standard operating protocols, richer metadata, shared repositories, and multi-metric reporting (e.g., precision and sensitivity), since accuracy alone varies widely and can be misleading under class imbalance [73]. Furthermore, there is a need of open, versioned libraries spanning weathering states, additives/pigments, biofilms, and matrices, with paired chemistry and morphology labels and clear guidance for calibration transfer [34, 72].

View Article Online
DOI: 10.1039/D5EN01084E

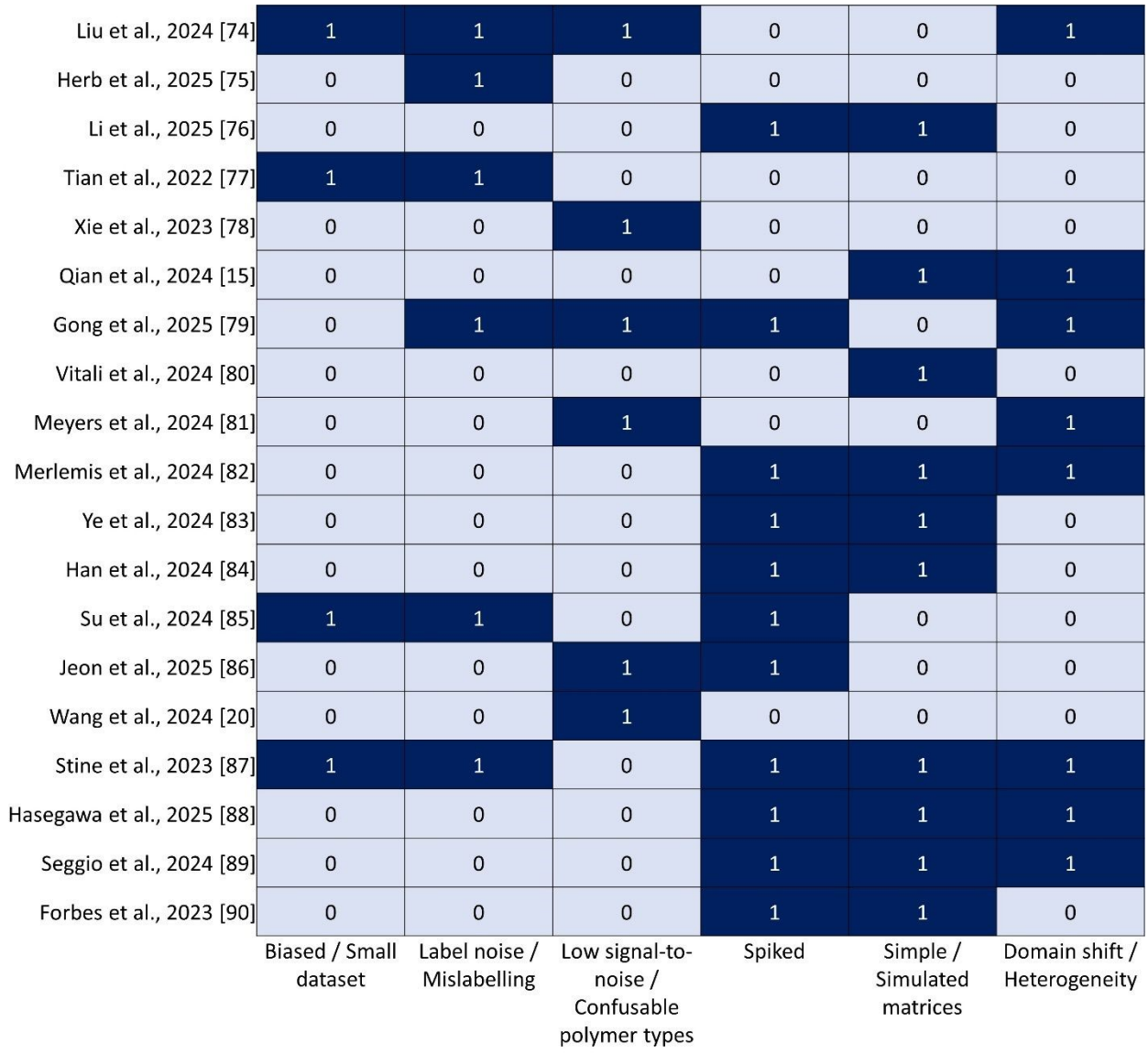

Figure 5 | Risk landscape summarizing limitations and deployment context across machine learning assisted analytical studies of waterborne nano- and microplastics (Section 3). Absence of a flag (1 = flagged; 0 = not flagged) does not imply absence of risk, it may indicate the issue was untested or unreported. Categories: Biased/Small dataset: Training or test sets are small, imbalanced, or skewed by polymer, size, weathering, or matrix; Label noise/Mislabelling: Known or suspected mis-annotations by human or database errors; Low signal-to-noise/Confusable polymer types: Weak signals or overlapping signatures leading to class confusion (e.g., PE vs PTFE; plastics vs organics); Spiked: Performance demonstrated on standard or lab-generated plastics

View Article Online
DOI: 10.1039/D5EN01084E

rather than original environmental nano- and microplastics; Simple/Simulated matrices: No validation in real environmental waters (e.g., only spiked tap waters, artificial seawater, and lab suspensions); Domain shift/Heterogeneity: Performance sensitive to real-word variabilities (e.g., weathering, additives, and biofilms) and to shifts across instruments and matrices.

In addition, pre-processing is decisive for model robustness. In spectral acquisition and downstream analysis, baseline correction, denoising/cosmic-ray removal, spectral windowing/derivatives, and dimensionality reduction (e.g., PCA) determine both performance and runtime. When tuned properly, PCA can deliver large speedups with minimal information loss. For example, pairing PEER with a random forest stabilized low-SNR Raman spectra [78], while fingerprint-windowed CNNs accelerated mapping at short dwell times [79]. Given pervasive domain shift (i.e., instrument, substrate, and matrix differences), safeguards such as transfer learning, calibrated uncertainty with abstention, and out-of-distribution checks are essential, particularly for confusable polymer pairs noted in spectroscopy studies [15, 78, 79]. Finally, researchers emphasize interpretability and physics-aware cues, and note that with sound pre-processing, simpler spectral models can rival heavier architectures while being easier to validate and deploy [20, 34, 71, 87, 90].

3.5.2 Nanoscale frontier and field deployment

Nanoplastic detection remains the most challenging frontier compared with microplastic analysis. Beyond inherent analytical limitations, weak or shifted peaks, small cross-sections, and background interference hinder single-particle identification, underscoring the need for tailored pre-processing, denoising, and data fusion [34]. SRS platform achieved detection below 100 nm yet revealed compositional and morphological heterogeneity that complicates spectral matching [15], while AI-assisted nano-DIHM required size corrections as features approached diffraction and reconstruction limits [20]. Accordingly, researchers call for nanoplastic focused databases, improved signal-to-noise approaches, and rigorous validation of substrate/enhancement strategies [34]. In parallel, edge deployment (e.g., smartphone fluorescence with on-device models [83]) is

View Article Online
DOI: 10.1039/D5EN01084E

becoming feasible. However, researchers caution that calibration transfer, drift management, and environmental interferences must be engineered alongside the analytics, and human oversight remains essential as systems transition to routine monitoring [71, 72].

4. Fate and transport models of waterborne nano- and microplastics

The numerical modelling of nanoplastic fate and transport remains in its early stages compared with that of microplastics, primarily because the dominant governing processes differ across scales. At the nanoscale, particle behaviour is controlled by Brownian motion, molecular diffusion, and surface-related interactions [91]. In contrast, at the microscale, transport is dominated by physical processes such as gravitational settling, hydrodynamic drag, shear-induced transport, and inertial dynamics, which are strongly influenced by particle size, shape, and density, as well as interactions with the surrounding fluid and other particles. These mechanisms result in distinct transport behaviours across different particle size classes [92, 93].

4.1 Existing Models for Microplastic Studies

The transport of microplastics in water is primarily described by the advection-diffusion equation, which forms the mathematical foundation of most fate and transport models. Numerical solutions to this equation enable the prediction of the spatial and temporal evolution of particle concentrations and trajectories. Because water acts as the carrier medium, hydrodynamic parameters, including flow velocity, water depth, turbulence intensity, and density stratification, must be prescribed. Consequently, fate and transport models are typically coupled with hydrodynamic solvers such as Delft3D [94], MIKE 21 [95], TELEMAC [96], or computational fluid dynamics (CFD) models such as OpenFOAM [93], which compute the detailed flow fields and turbulence characteristics required for particle transport simulations [97-102].

In the context of numerical modelling, the advection-diffusion equation can be solved using either Eulerian or Lagrangian approaches. Eulerian models represent particle concentrations as continuous fields that evolve over space and time. They are particularly

View Article Online
DOI: 10.1039/D5EN01084E

suitable for large-scale or long-term simulations, such as those of coastal, estuarine, or riverine systems, where the objective is to capture overall concentration patterns rather than the trajectories of individual particles. Processes such as aggregation, degradation, fragmentation, and sedimentation can be incorporated through source–sink or reaction terms in the governing equations [93, 101, 103].

Lagrangian models, in contrast, track the trajectories of individual particles or particle parcels as they move through the flow field. This approach explicitly accounts for variability in particle properties, such as size, density, and shape, and captures stochastic particle-flow interactions. The Lagrangian framework is particularly effective for resolving three-dimensional transport, deposition, and resuspension processes in dynamic flow environments [104, 105].

Because microplastics behave as discrete particles with negligible molecular diffusion and are insoluble, and because modelling objectives often focus on particle-scale metrics, including residence time, accumulation zones, and transport pathways, the Lagrangian or particle-tracking approach has become the dominant framework in the literature. Recent advances in parallel and graphics processing unit (GPU)-based computing have further reinforced this trend by significantly improving computational efficiency and enabling the simulation of millions of particles.

Eulerian models however are generally impractical for simulating large domains or long time periods because the governing equations must be solved for all computational mesh nodes at every time step, even in regions where particles are absent, making them computationally inefficient for sparse particle distributions. The Lagrangian framework, on the other hand, allows direct computation of integral transport parameters that are critical for understanding environmental behaviour, such as settling, residence time, accumulation zones, and source-sink connectivity [99, 106].

The modelling capabilities and methodologies, particularly for kinematic or advection-diffusion based approaches, which remain the most widely used, have been comprehensively reviewed in several recent studies [93, 102, 107]. Despite variations in

View Article Online
DOI: 10.1039/D5EN01084E

the employed hydrodynamic models or minor differences in numerical formulations, these models are fundamentally governed by the same physical principles described above.

Beyond kinematic models, more advanced dynamic approaches solve the full particle equation of motion to represent complex particle dynamics. These models explicitly incorporate forces such as drag, gravity, buoyancy, and lift, thereby resolving behaviours such as settling, resuspension, inertial lag, particle transformation, and inter-particle interactions [103, 108]. Dynamic models solve a force balance for each individual particle, enabling explicit representation of a wide range of physical and physicochemical forces acting on microplastics, including inter-particle collisions, particle-bed interactions, electrostatic and surface forces, and changes in particle properties such as size, density, and surface roughness based on ambient environment properties [109].

Such detailed models provide valuable insights into mechanisms governing microplastic transport, aggregation, and retention, particularly in near-bed regions and sediment-water interfaces [103, 110, 111]. For instance, vertical transport plays a crucial role in determining microplastic residence time and spatial distribution. In kinematic models, this effect can only be incorporated indirectly through empirical settling formulations derived from laboratory experiments. In two-dimensional frameworks, settling velocity is often estimated from empirical relationships based on particle density and shape, whereas in three-dimensional models, it is represented as the resultant of the water's vertical velocity and the particle's terminal settling velocity. These formulations provide an approximate description of vertical motion [93, 108, 112].

The main challenge of computer models lies in the representation of complex environmental processes, including transformation (e.g., biofouling, UV weathering, and aggregation [113-117]), turbulent dispersion [118-120], settling velocity [121-123], and sedimentation/resuspension [124-126]. Representing these processes in simplified yet physically meaningful ways, so they can be feasibly incorporated into numerical models without excessive computational cost, remains a major modelling limitation.

In this regard, progresses in analytical advances play a critical role. High-quality observational data obtained from these techniques provide essential information for

View Article Online
DOI: 10.1039/D5EN01084E

parameterizing key processes and improving model calibration and validation, ultimately enhancing the predictive accuracy of numerical simulations.

4.2 Opportunities and Challenges in Modelling Nanoplastic Particles

Fate and transport models that explicitly represent the underlying physical and chemical mechanisms for nanoplastics in natural waters are still sparse. Compared with microplastics, nanoscale plastic particles are governed by Brownian diffusion, rapid homo- and hetero-aggregation, and fast-evolving surface chemistry such as eco-coronas and photo or thermal aging. Mesocosm studies already point to strong retention and sediment coupling of gold-doped PS nanoparticles in relatively simple freshwater systems [127]. Meanwhile, electrolyte composition and natural organic matter can either stabilize suspensions or promote aggregation, depending on ionic conditions and particle aging [128, 129]. These processes modify particle size, density, and surface charge, which in turn control advection-diffusion, water-sediment exchange, and bioavailability [38]. Improving model feasibility therefore requires careful treatment of these coupled transformations (Figure 6).

For bulk transport of primary nanoplastics, longitudinal displacement is governed by advection, while cross-sectional mixing is typically set by shear and turbulence. Within this hydrodynamic regime, Brownian motion dominates the microscale collisions that initiate aggregation. A standard 2D/3D advection-diffusion-reaction (ADR) framework is thus appropriate, with advection and turbulent diffusion resolving transport, and Stokes-Einstein Brownian diffusion informing both collision kernels and near-interface mass transfer [130]. Model realism depends on accurate hydrological and geochemical inputs and on regularly updating particle physicochemical parameters as they evolve. Interactions with natural colloids (e.g., clays, metal oxides, and biogenic particles) and weathering from light-driven oxidation shift particle size and surface chemistry, often increasing particle attachment efficiency. As attachment efficiency is also sensitive to salinity, divalent cations, and natural organic matter, these factors together determine nanoplastic fate and transport [131-133]. Gravitational settling of primary nanoplastics

View Article Online
DOI: 10.1039/D5EN01084E

can usually be neglected at first and activated dynamically once aggregates grow to microscale sizes [134, 135].

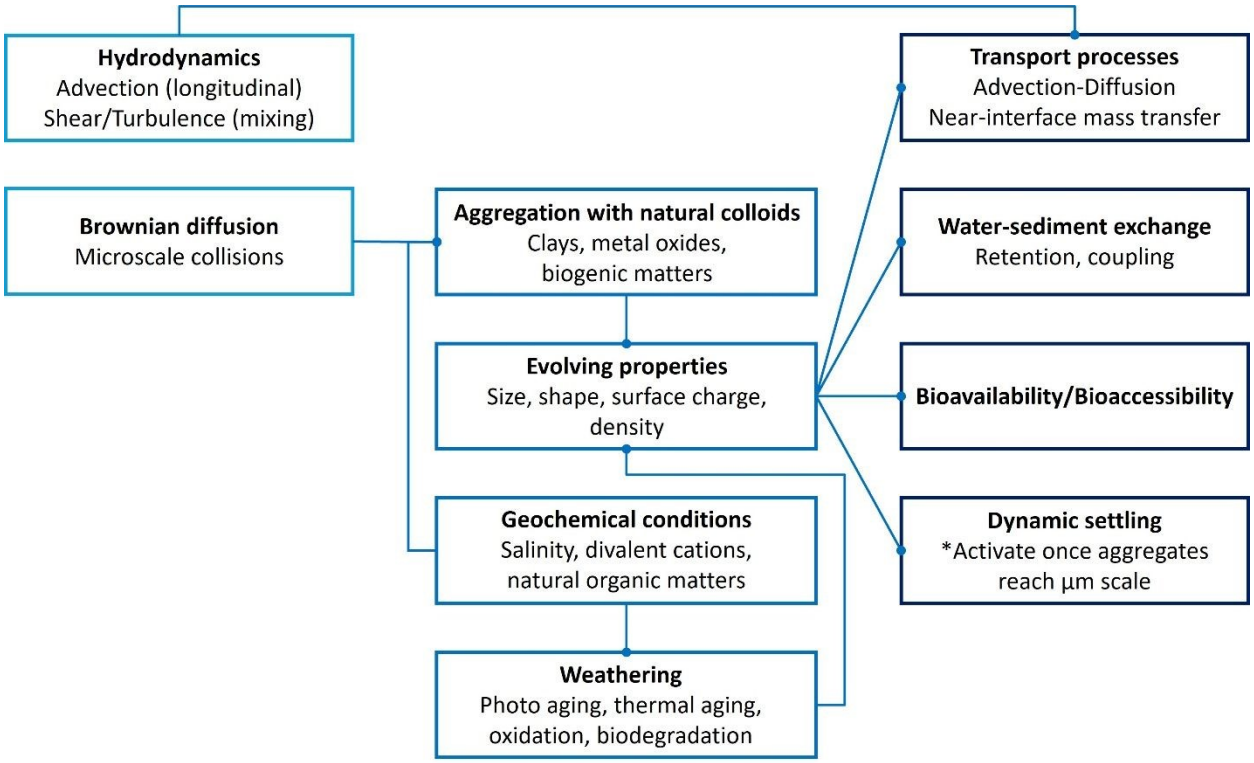

Figure 6 | Mechanistic factors on nanoplastic fate and transport in natural waters for model simulations. Hydrodynamics and Brownian collisions set encounter rates (left). Transformations, aggregation with natural colloids and weathering, together with geochemical factors update particle properties (middle). The evolving properties regulate advection-diffusion-reaction transport and near-interface mass transfer, water-sediment exchange, and bioavailability (right). Settling of primary nanoplastics is neglected initially and activated when aggregates reach micrometre scale. Arrows indicate influence.

Several tools from engineered nanomaterial modelling offer practical starting points. The spatially explicit NanoDUFLOW river model and the multimedia SimpleBox4Nano model both represent aggregation with natural solids and track particle size distributions [134, 136]. With appropriate re-parameterization for plastics, such as no dissolution and buoyancy and density that evolve with sorption and corona formation, these tools can be

View Article Online
DOI: 10.1039/D5EN01084E

adapted to nanoplastics. As a screening complement across nano- and microplastics, SimpleBox4Plastic supports scenario analysis for nanoplastics in natural waters [137].

5. Future Directions

Safeguarding water quality in the age of nanoplastics demands a decisive shift from isolated demonstrations to interoperable, rigorously validated, and scalable systems that seamlessly integrate measurements, models, and management. Building on the advances discussed in this review, we chart a practical near-term agenda anchored in mutually reinforcing priorities designed to accelerate innovation and real-world impact.

5.1 Converging on interoperable protocols and reporting standards

Fragmented approaches to sampling, extraction, spectral preprocessing, and classification undermine comparability across studies and slow the adoption of robust methods. Without minimum reporting standards, uncertainty remains opaque, and meta-analyses lack reliability, creating barriers to evidence-based regulation.

To close this gap, the scientific community should establish a Minimum Information for Reporting Nano- and Microplastic Analytics checklist aligned with ISO 24187 and emerging guidance from the European Committee for Standardization (CEN) and ISO. This checklist should, where applicable, specify sample origin, pretreatment, size and shape bins, polymer classes, and quality control measures, including field and procedural blanks, recovery surrogates, and detection and quantification limits for each polymer and matrix. It should also include model architecture and training data for machine learning approaches, as well as methods for uncertainty quantification. Standardized reporting is critical for translating research into actionable policies, enabling regulators to set enforceable limits, monitor compliance, and protect ecosystems and public health in the face of growing nanoplastic risks.

5.2 Environmentally realistic reference materials and interlaboratory trials

There are key challenges associated with developing environmentally realistic reference materials and conducting interlaboratory trials. For example, validation using pristine,

View Article Online
DOI: 10.1039/D5EN01084E

monodisperse beads often overestimates analytical performance and obscures failure modes that arise with weathered polymers, additives, biofilms, and heterogeneous matrices. This discrepancy limits the reliability of current detection and quantification methods for nano- and microplastics in real-world environments. To address these challenges, we propose two systematic objectives: (a) develop and certify environmentally realistic reference materials that accurately reflect actual environmental conditions; and (b) conduct blinded interlaboratory comparisons to benchmark analytical methods under realistic scenarios.

For the production of reference materials, we recommend generating size-fractionated nano- and microplastics that incorporate controlled ultraviolet, thermal, and oxidative weathering, as well as representative additives and eco-coronas. These materials should be embedded in matrices representative of freshwater, estuarine, wastewater, and drinking water environments. Interlaboratory trials should implement blinded comparisons across spectroscopy, mass spectrometry, imaging, and electrochemical techniques. Key performance metrics to be reported include recovery rates, false positive and false negative rates, size-dependent bias, and robustness to matrix variability, among others. By pursuing these objectives, we anticipate several positive outcomes: (a) standardized, certified reference materials tailored to realistic environmental conditions; (b) comprehensive performance benchmarks for analytical methods; and (c) improved reliability and reproducibility in the detection of nano- and microplastics.

5.3 Shared datasets and comparisons for machine learning assisted studies

Comparisons across machine learning assisted studies remain challenging when groups rely on different datasets and scoring rules. A practical solution emphasizes shared datasets, shared tasks, and standardized reporting. Community datasets for IR, Raman, SERS, SRS, O-PTIR, and AFM-IR, along with particle-level images are needed. Each record should include accurate labels and a brief note on sample origin and preparation. Upon publication, associated data and code should be deposit in open repositories to enable reuse.

View Article Online
DOI: 10.1039/D5EN01084E

Common tasks should include polymer identification, size bin classification, weathering stage recognition, and out-of-scope detection, with fixed train/validation/test splits. Additional challenge subsets spanning instruments, matrices, and weathering states should be considered to assess robustness under real-world variation. Baseline, reproducible workflows with unit tests and clear documentation should serve as reference points that others can rerun.

Reporting should cover both standard scores (e.g., accuracy and precision) and calibrated uncertainty (e.g., calibration curves and prediction intervals), allowing readers to evaluate predictions alongside their associated confidence levels.

5.4 Routine uncertainty quantification and traceability

Accurate characterization of microplastic contamination and polymeric material distribution is critical for informed decision-making in product design, regulatory permitting, and environmental remediation. These decisions increasingly require defensible, quantitative estimates of concentration, flux, and source attribution that are expressed through credible intervals rather than single-point values. Point estimates, while common, fail to capture the inherent variability and uncertainty associated with environmental sampling and analytical workflows, leading to potential misinterpretation of risk and exposure.

To address these challenges, comprehensive end-to-end uncertainty quantification frameworks are essential. Such frameworks must propagate error across all stages of analysis, beginning with sampling and extending through extraction losses, instrumental signal-to-noise limitations, and classification ambiguity. This propagation ensures that uncertainty is not underestimated when translating raw measurements into particle-based and mass-based concentration estimates. Sampling uncertainty, in particular, must explicitly account for spatial and temporal variability and recovery efficiency, given the heterogeneity of environmental matrices and the dynamic nature of contaminant distributions.

View Article Online
DOI: 10.1039/D5EN01084E

Standardization of reporting practices is equally critical for comparability and reproducibility across studies. Confidence intervals at defined levels should accompany particle counts and mass estimates, while polymer-resolved misclassification matrices should be incorporated to quantify classification error. Furthermore, sensitivity analyses evaluating the influence of preprocessing choices on final outcomes are necessary to identify methodological biases and improve robustness. Establishing these rigorous protocols will not only enhance scientific transparency but also strengthen regulatory frameworks and risk assessments, ultimately supporting evidence-based strategies for pollution mitigation and sustainable material management.

5.5 Field testbeds that connect sensors, analytics, and models to decisions

To move beyond laboratory demonstrations, we propose establishing real-world testbeds that integrate continuous monitoring, automated data processing, and catchment-scale modelling into a single operational pipeline. These pilots will demonstrate how advanced sensing and analytics can deliver actionable insights for water safety and resource management. Field instruments will stream data through open interfaces into validated analysis workflows, which then feed hydrological and water-quality models. The combined system will produce decision-ready outputs, including particle number and mass fluxes, removal efficiency across treatment steps, threshold exceedance frequency, and event detection, accompanied by calibrated uncertainty and confidence levels.

This end-to-end integration moves beyond fragmented research toward deployable solutions. Testbeds will be implemented along critical pathways, from wastewater outfalls to downstream drinking-water intakes across diverse contexts, including low-resource settings. Each deployment will include side-by-side confirmation with reference methods, routine checks on false positives and false negatives, and stress testing under storms, maintenance upsets, and seasonal change. Performance will be judged on uptime, latency from sample to result, accuracy with quantified uncertainty, false-alarm rate, cost per decision, and ease of integration with utility workflows. Outputs will include shared data schemas, reference implementations of the analysis workflows, and concise playbooks that show how to choose methods for screening, compliance monitoring,

View Article Online
DOI: 10.1039/D5EN01084E

incident response, and product stewardship. By proving the full measurement-to-action pathway in the field, these testbeds will convert scattered advances into tools that operators and regulators can deploy at scale, accelerating progress toward resilient water systems and safeguarding public health.

5.6 Translation of science to policy, procurement, and practice

Ongoing treaty negotiations and national or regional regulations require practical, standardized metrics and methods that authorities and industry can implement effectively. It is important to link analytical results to policy-relevant indicators, polymer-resolved particle counts and mass fluxes, removal efficiency with its uncertainty, the frequency of thresholds exceedances, and the confidence in source attribution. Short guidance should be co-developed with regulators, utilities, and industry on choosing methods for screening, compliance monitoring, incident response, and product stewardship, with decision trees keyed to matrix, concentration range, and available resources. Build in equity and ethics by ensuring reference materials and test sets reflect low-resource contexts and by supporting capacity building and open tools to avoid dependence on a single technology.

Together these steps shift the field from disparate demonstrations to a coherent, reproducible, and scalable evidence base. By making methods work together through common standards, the community can ensure that rapid advances in nanoscale analytical capability, machine learning, and modelling translate into timely and trusted guidance for protecting water quality across the plastic life cycle.

5.7 New technologies, improved methods, more accurate analyses, enhanced models, and the use of AI for predicting hot spots and advancing remediation strategies

Rapid advancements in technology are transforming environmental monitoring and remediation. To meet growing regulatory and sustainability demands, new tools and methods must deliver higher accuracy, predictive capabilities, and adaptive solutions. Innovations in nano-sensor design, sampling techniques, and laboratory instrumentation

View Article Online
DOI: 10.1039/D5EN01084E

are enabling ultra-trace detection and real-time monitoring. These improvements reduce measurement uncertainty and provide more reliable data for compliance and risk assessment.

Next-generation models now integrate physical, chemical, and biological processes to better represent complex environmental systems. These models support scenario testing, improved forecasting, and more accurate estimation of pollutant transport and transformation.

Artificial Intelligence (AI) is enhancing decision-making by leveraging high-resolution data and predictive analytics to enable proactive interventions. AI-driven prioritization ensures efficient allocation of monitoring and remediation resources. Open-source tools and capacity-building initiatives can help prevent technological monopolies and support low-resource regions.

Yet, significant challenges remain. Ethical and social concerns include bias and discrimination, which can emerge from demographic, geographic, and linguistic skews in training data and evaluation benchmarks, causing models to reflect dominant cultural norms and to underperform for underrepresented groups. Additional risks include privacy violations, limited transparency, and potential job displacement due to labour market shifts. Technical challenges involve robustness, reliability, security risks, and generalization limits, as many AI models struggle to perform consistently across diverse contexts without retraining. Environmental impacts are also notable, as the high energy consumption contributes to carbon emissions and ecological degradation.

Therefore, detection and remediation approaches must be carefully evaluated. It is worth remembering that technologies initially developed for sustainability, such as plastics or fluorochlorocarbons, later revealed unintended consequences, including ozone depletion. Similarly, the rapid expansion of industrial infrastructure can trigger unintended environmental burdens, such as water depletion, further exacerbating water scarcity in regions already under hydrologic stress. Anthropogenic activities continue to affect climate and planetary health.

View Article Online
DOI: 10.1039/D5EN01084E

AI must be applied responsibly and with purpose, not in vain.

Glossary of terms

ADR: Advection-Diffusion-Reaction
AF4: Asymmetric Flow Field-Flow Fractionation
AFM: Atomic Force Microscopy
BSA: Bovine Serum Albumin
CEN: European Committee for Standardization
CPE: Carbon Paste Electrode
CSRR: Complementary Split Ring Resonator
DAD: Diode-Array Detector
DEP: Dielectrophoresis
EC: Electrochemical
EDX: Energy Dispersive X-Ray
EIS: Electrochemical Impedance Spectroscopy
FePDA: Iron-Doped Polydopamine
FLA: Fluorescence Lifetime Analysis
HCA: Hierarchical Custer Analysis
HDPE: High-Density Polyethylene
IPD: Integrated Passive Device
IR: Infrared
ISO: International Organization for Standardization
LDPE: Low-Density Polyethylene
LFOC: Laser-Backscattered Fiber-Embedded Optofluidic Chip
LIBD: Laser-Induced Breakdown Detection
LOD: Limit of Detection
L-PHA: L-Phenylalanine
MALS: Multi-Angle Light Scattering
PCB: Printed Circuit Board
PE: Polyethylene
PEC: Photoelectrochemical
PEG: Polyethylene Glycol
PET: Polyethylene Terephthalate
PLA: Polylactic Acid
PMMA: Polymethyl Methacrylate
PP: Polypropylene
PS: Polystyrene
PVA: Polyvinyl Alcohol
PVC: Polyvinyl Chloride
Py-GC-MS: Pyrolysis-Gas Chromatography Mass Spectrometry
QCM: Quartz Crystal Microbalance
SEM: Scanning Electron Microscopy
SERS: Surface-Enhanced Raman Spectroscopy
SPR: Surface Plasmon Resonance
SSBD: Shrinking Surface Bubble Deposition
TD-PTR-MS: Thermal-Desorption Proton-Transfer-Reaction Mass Spectrometry
UV-vis: Ultraviolet-Visible
ZIF: Zeolitic Imidazolate Framework

View Article Online
DOI: 10.1039/D5EN01084E

References

1. Science Museum, The age of plastic: From Parkesine to pollution, Chemistry, 2019, available at: https://www.sciencemuseum.org.uk/objects-and-stories/chemistry/age-plastic-parkesine-pollution (accessed 10 Feb 2026).
2. UNEP, Plastic Pollution, 2025, available at: https://www.unep.org/plastic-pollution (accessed 10 Feb 2026).
3. J. E. Sonke, et al., Global environmental plastic dispersal under OECD policy scenarios toward 2060, Sci. Adv., 2025, 11, 16, eadu2396, DOI: 10.1126/sciadv.adu2396.
4. OECD, Global plastics outlook: Policy scenarios to 2060, OECD Publishing, Paris, 2022, DOI: 10.1787/aa1edf33-en.
5. UNEP, Intergovernmental negotiating committee to develop an international legally binding instrument on plastic pollution, including in the marine environment (Chair's Text), 1 Dec 2024, available at: https://www.unep.org/inc-plastic-pollution/session-5 (accessed 10 Feb 2026).
6. ISO, ISO 24187:2023: Principles for the analysis of microplastics present in the environment, International Organization for Standardization, 2023.
7. N. B. Hartmann, et al., Are we speaking the same language? Recommendations for a definition and categorization framework for plastic debris, Environ. Sci. Technol., 2019, 53, 3, 1039–1047, DOI: 10.1021/acs.est.8b05297.
8. W. Cowger, et al., Reporting guidelines to increase the reproducibility and comparability of research on microplastics, Appl. Spectrosc., 2020, 74, 9, 1066–1077, DOI: 10.1177/0003702820930292.
9. S. Belz, et al., Analytical methods to measure microplastics in drinking water, Publications Office of the European Union, Luxembourg, 2024, JRC136859, DOI:10.2760/109944.
10. R. Permana, S. Chakraborty and E. Valsami-Jones, Nanoplastics in aquatic environments: The hidden impact of aging on fate and toxicity, Environ. Chem. Ecotoxicol., 2025, 7, 429–444, DOI: 10.1016/j.enceco.2025.02.007.
11. C. B. Prater, M. Kansiz and J.-X. Cheng, A tutorial on optical photothermal infrared (O-PTIR) microscopy, APL Photonics, 2024, 9, 9, 091101, DOI: 10.1063/5.0219983.
12. Y. Li, et al., Identification and quantification of nanoplastics (20–1000 nm) in a drinking water treatment plant using AFM-IR and Pyr-GC/MS, J. Hazard. Mater., 2024, 463, 132933, DOI: 10.1016/j.jhazmat.2023.132933.
13. S. L. Belontz, et al., Combining submicron spectroscopy techniques (AFM-IR and O-PTIR) to detect and quantify microplastics and nanoplastics in snow from a Utah ski resort, Environ. Sci. Technol., 2025, 59, 26, 13362–13373, DOI: 10.1021/acs.est.4c12170.
14. D. Xie, et al., Identification of microplastics and nanoplastics in environmental water by AFM-IR, Anal. Chim. Acta, 2025, 1354, 343992, DOI: 10.1016/j.aca.2025.343992.
15. N. Qian, et al., Rapid single-particle chemical imaging of nanoplastics by SRS microscopy, Proc. Natl. Acad. Sci. U. S. A., 2024, 121, 3, e2300582121, DOI: 10.1073/pnas.2300582121.
16. Y. Xu, et al., Identification and quantification of nanoplastics in surface water and groundwater by pyrolysis gas chromatography–mass spectrometry, Environ. Sci. Technol., 2022, 56, 8, 4988–4997, DOI: 10.1021/acs.est.1c07377.

View Article Online
DOI: 10.1039/D5EN01084E

17. J. Dalmau-Soler, et al., Routine method for the analysis of microplastics in natural and drinking water by pyrolysis coupled to gas chromatography–mass spectrometry, J. Chromatogr. A, 2024, 1730, 465153, DOI: 10.1016/j.chroma.2024.465153.
18. D. Materić, et al., Presence of nanoplastics in rural and remote surface waters, Environ. Res. Lett., 2022, 17, 054036, DOI: 10.1088/1748-9326/ac68f7.
19. S. Ten Hietbrink, et al., Nanoplastic concentrations across the North Atlantic, Nature, 2025, 643, 8071, 412–416, DOI: 10.1038/s41586-025-09218-1.
20. Z. Wang, et al., Nanoplastics in water: Artificial intelligence-assisted 4D physicochemical characterization and rapid in situ detection, Environ. Sci. Technol., 2024, 58, 20, 8919–8931, DOI: 10.1021/acs.est.3c10408.
21. Z. Wang, N. K. Saade and P. A. Ariya, Advances in ultra-trace analytical capability for micro/nanoplastics and water-soluble polymers in the environment: Fresh falling urban snow, Environ. Pollut., 2021, 276, 116698, DOI: 10.1016/j.envpol.2021.116698.
22. Y. Liu, et al., Detecting small microplastics down to 1.3 μm using large area ATR-FTIR, Mar. Pollut. Bull., 2024, 198, 115795, DOI: 10.1016/j.marpolbul.2024.115795.
23. I. Tarhan and H. M. Kestek, Investigation of new analysis methods for simultaneous and rapid identification of five different microplastics using ATR-FTIR spectroscopy and chemometrics, Environ. Pollut., 2024, 362, 125043, DOI: 10.1016/j.envpol.2024.125043.
24. F. O. Sefiloğlu, et al., Comparative microplastic analysis in urban waters using μ-FTIR and Py-GC-MS: A case study in Amsterdam, Environ. Pollut., 2024, 351, 124088, DOI: 10.1016/j.envpol.2024.124088.
25. J. Yang, et al., Microplastics in different water samples (seawater, freshwater, and wastewater): Methodology approach for characterization using micro-FTIR spectroscopy, Water Res., 2023, 232, 119711, DOI: 10.1016/j.watres.2023.119711.
26. S. Samandra, et al., Microplastic contamination of an unconfined groundwater aquifer in Victoria, Australia, Sci. Total Environ., 2022, 802, 149727, DOI: 10.1016/j.scitotenv.2021.149727.
27. J. Hansen, et al., Quantification and characterization of microplastics in surface water samples from the Northeast Atlantic Ocean using laser direct infrared imaging, Mar. Pollut. Bull., 2023, 190, 114880, DOI: 10.1016/j.marpolbul.2023.114880.
28. X. Shi, et al., Capturing, enriching and detecting nanoplastics in water based on optical manipulation, surface-enhanced Raman scattering and microfluidics, Nat. Water, 2025, 3, 4, 449–460, DOI: 10.1038/s44221-025-00417-8.
29. L. Xie, et al., Strategies and challenges of identifying nanoplastics in environment by surface-enhanced Raman spectroscopy, Environ. Sci. Technol., 2023, 57, 1, 25–43, DOI: 10.1021/acs.est.2c07416.
30. D. Schymanski, et al., Analysis of microplastics in water by micro-Raman spectroscopy: Release of plastic particles from different packaging into mineral water, Water Res., 2018, 129, 154–162, DOI: 10.1016/j.watres.2017.11.011.
31. C. F. Araújo, et al., Identification of microplastics using Raman spectroscopy: Latest developments and future prospects, Water Res., 2018, 142, 426–440, DOI: 10.1016/j.watres.2018.05.060.

View Article Online
DOI: 10.1039/D5EN01084E

32. D. D. Pramanik, P. Kay and F. M. Goycoolea, A rapid and portable fluorescence spectroscopy staining method for the detection of plastic microfibers in water, Sci. Total Environ., 2024, 908, 168144, DOI: 10.1016/j.scitotenv.2023.168144.
33. B. Nguyen and N. Tufenkji, Single-particle resolution fluorescence microscopy of nanoplastics, Environ. Sci. Technol., 2022, 56, 10, 6426–6435, DOI: 10.1021/acs.est.1c08480.
34. L. Xie, et al., Machine learning advancements and strategies in microplastic and nanoplastic detection, Environ. Sci. Technol., 2025, 59, 18, 8885–8899, DOI: 10.1021/acs.est.4c11888.
35. M. M. Khanam, M. K. Uddin and J. U. Kazi, Advances in machine learning for the detection and characterization of microplastics in the environment, Front. Environ. Sci., 2025, 13, 1547798, DOI: 10.3389/fenvs.2025.1573579.
36. B. R. Coleman, An introduction to machine learning tools for the analysis of microplastics in complex matrices, Environ. Sci.: Processes Impacts, 2025, 27, 1, 10–23, DOI: 10.1039/D4EM00605D.
37. Y. Wang, Z. Gu and X. Chen, Modeling of heteroaggregation driven buoyant microplastic settling: Interaction with multiple clay particles, Sci. Total Environ., 2025, 959, 178169, DOI: 10.1016/j.scitotenv.2024.178169.
38. A. Pradel, C. Catrouillet and J. Gigault, The environmental fate of nanoplastics: What we know and what we need to know about aggregation, NanoImpact, 2023, 29, 100453, DOI: 10.1016/j.impact.2023.100453.
39. R. Zhang, et al., Fate models of nanoparticles in the environment: A critical review and prospects, Environ. Sci.: Nano, 2025, 12, 7, 3394–3412, DOI: 10.1039/D5EN00342C.
40. H. Yang, et al., A review of eco-corona formation on micro/nanoplastics and its effects on stability, bioavailability, and toxicity, Water, 2025, 17, 8, 1493, DOI: 10.3390/w17081124.
41. S. Grumelot, et al., Identification of pristine and protein corona coated micro- and nanoplastic particles with a colorimetric sensor array, ACS Omega, 2024, 9, 37, 39188–39194, DOI: 10.1021/acsomega.4c06166.
42. F. Hu, et al., A single-atom nanozyme-enabled strategy for rapid, visual, and real-time detection of polystyrene nanoplastics in water, J. Environ. Chem. Eng., 2024, 12, 6, 114541, DOI: 10.1016/j.jece.2024.114541.
43. T. S. S. K. Naik, et al., Biomimetic iron-doped polydopamine sensor for selective detection of polystyrene nanoplastics, ACS ES&T Water, 2025, 5, 6, 3241–3250, DOI: 10.1021/acsestwater.5c00090.
44. W. Y. Lim, et al., Electrophoresis and quartz crystal microbalance instrumentation to sense nanoplastics in water, Anal. Chem., 2024, 96, 49, 19213–19219, DOI: 10.1021/acs.analchem.4c05466.
45. Y.-X. Wang, et al., Integrated passive sensing chip for highly sensitive and reusable detection of differential-charged nanoplastics concentration, ACS Sens., 2023, 8, 10, 3862–3872, DOI: 10.1021/acssensors.3c01406.
46. W. Guo, et al., An electrochemiluminescence-activated amphiphilic perylene diimide probe: enabling highly sensitive and selective detection of polypropylene nanoplastics in the environment, Anal. Chem., 2025, 97, 19, 10218–10226, DOI: 10.1021/acs.analchem.4c07054.

View Article Online
DOI: 10.1039/D5EN01084E

47. Z. Xiao, et al., Smart and accurate detection of nanoplastics in aquatic environments by photoelectrochemical-electrochemical dual-mode portable sensor, Sens. Actuators B: Chem., 2024, 420, 136483, DOI: 10.1016/j.snb.2024.136483.
48. C. Kim, et al., Epizoochory-inspired universal nanoplastic sensor, Chem. Eng. J., 2025, 519, 165434, DOI: 10.1016/j.cej.2025.165434.
49. M. Urso, et al., Trapping and detecting nanoplastics by MXene-derived oxide microrobots, Nat. Commun., 2022, 13, 3573, DOI: 10.1038/s41467-022-31161-2.
50. E. S. Yu, et al., Real-time underwater nanoplastic detection beyond the diffusion limit and low Raman scattering cross-section via electro-photonic tweezers, ACS Nano, 2023, 17, 3, 2114–2123, DOI: 10.1021/acsnano.2c07933.
51. Z. Geng, et al., Visible-light-sensitive microrobots using H_2O as fuel for highly efficient capture and precise detection of nanoplastics, J. Hazard. Mater., 2024, 479, 135731, DOI: 10.1016/j.jhazmat.2024.135731.
52. S. Moon, et al., Direct observation and identification of nanoplastics in ocean water, Sci. Adv., 2024, 10, 4, eadh1675, DOI: 10.1126/sciadv.adh1675.
53. Q. Yang, et al., Identification of trace polystyrene nanoplastics down to 50 nm by the hyphenated method of filtration and surface-enhanced Raman spectroscopy based on silver nanowire membranes, Environ. Sci. Technol., 2022, 56, 15, 10818–10828, DOI: 10.1021/acs.est.2c02584.
54. H. Ye, et al., Integrating metal-phenolic networks-mediated separation and machine learning-aided surface-enhanced Raman spectroscopy for accurate nanoplastics quantification and classification, ACS Nano, 2024, 18, 38, 26281–26296, DOI: 10.1021/acsnano.4c08316.
55. H. Yang, et al., Electrochemical and surface-enhanced Raman scattering coupling for dual-mode sensing of nanoplastics, Anal. & Sens., 2025, DOI: 10.1002/anse.202500076.
56. I. Cârdan, et al., Blue micro-/nanoplastics abundance in the environment: a double threat as a Trojan horse for a plastic-Cu-phthalocyanine pigment and an opportunity for nanoplastic detection via micro-Raman spectroscopy, Environ. Sci.: Nano, 2025, 12, 4, 2357–2370, DOI: 10.1039/D4EN00820K.
57. M. Fadda, et al., Tracking nanoplastics in drinking water: a new frontier with the combination of dielectrophoresis and Raman spectroscopy, Microplast. Nanoplast., 2025, 5, 1, 24, DOI: 10.1186/s43591-025-00131-y.
58. M. Seggio, et al., A plasmonic gold nano-surface functionalized with the estrogen receptor for fast and highly sensitive detection of nanoplastics, Talanta, 2024, 267, 125211, DOI: 10.1016/j.talanta.2023.125211.
59. Y. Lu, et al., Rapid, sensitive, and non-destructive on-site quantitative detection of nanoplastics in aquatic environments using laser-backscattered fiber-embedded optofluidic chip, J. Hazard. Mater., 2024, 479, 135591, DOI: 10.1016/j.jhazmat.2024.135591.
60. M. N. Nguyen, et al., Quantification of nanoplastics and inorganic nanoparticles via laser-induced breakdown detection (LIBD), Small Methods, 2025, 9, e2402060, DOI: 10.1002/smtd.202402060.

View Article Online
DOI: 10.1039/D5EN01084E

61. S. Xiao, et al., Fast and portable fluorescence lifetime analysis for early warning detection of micro- and nanoplastics in water, Environ. Res., 2024, 244, 117936, DOI: 10.1016/j.envres.2023.117936.
62. H. Li, et al., Operando on-line monitoring of nanoplastics in real environmental water samples enabling an optical microfiber Mach–Zehnder interferometer, J. Environ. Chem. Eng., 2024, 12, 6, 114651, DOI: 10.1016/j.jece.2024.114651.
63. S. Guchhait, et al., A metal-insulator-metal waveguide-based plasmonic refractive index sensor for the detection of nanoplastics in water, Sci. Rep., 2024, 14, 21495, DOI: 10.1038/s41598-024-71874-6.
64. C. Adelantado, et al., Capillary electrophoresis as a complementary analytical tool for the separation and detection of nanoplastic particles, Anal. Chem., 2024, 96, 19, 7706–7713, DOI: 10.1021/acs.analchem.4c00822.
65. E. D. Okoffo and K. V. Thomas, Quantitative analysis of nanoplastics in environmental and potable waters by pyrolysis-gas chromatography-mass spectrometry, J. Hazard. Mater., 2024, 464, 133013, DOI: 10.1016/j.jhazmat.2023.133013.
66. H. Li, et al., An optimized multi-technique based analytical platform for identification, characterization and quantification of nanoplastics in water, Talanta, 2024, 272, 125800, DOI: 10.1016/j.talanta.2024.125800.
67. C. Rauert, et al., Assessing the efficacy of pyrolysis–gas chromatography–mass spectrometry for nanoplastic and microplastic analysis in human blood, Environ. Sci. Technol., 2025, 59, 4, 1984–1994, DOI: 10.1021/acs.est.4c12599.
68. C. Rauert, et al., Extraction and pyrolysis–GC–MS analysis of polyethylene in samples with medium to high lipid content, J. Environ. Expo. Assess., 2022, 1, 13, DOI: 10.20517/jeea.2022.04.
69. D. Ciornii, et al., Interlaboratory comparison reveals state of the art in microplastic detection and quantification methods, Anal. Chem., 2025, 97, 16, 8719–8728, DOI: 10.1021/acs.analchem.4c05403.
70. B. Ferreiro, et al., Microplastic mass estimation using two-dimensional chemical images from quantum-cascade laser-based infrared spectrometers, Anal. Chem., 2025, 97, 44, 24458–24467, DOI: 10.1021/acs.analchem.5c04003.
71. K. Mathur, et al., Computational approaches for identification of micro/nano-plastic pollution, in Global Impacts of Micro- and Nano-Plastic Pollution, 2024, 99–122, DOI: 10.4018/979-8-3693-3447-8.ch005.
72. B. Zhao, et al., Advancing microplastic analysis in the era of artificial intelligence: from current applications to the promise of generative AI, Nexus, 2024, 1, 4, 100043, DOI: 10.1016/j.ynexs.2024.100043.
73. H. Huang and J. Ullah, Application of artificial intelligence in the analysis of microplastics, in Analysis of Microplastics and Nanoplastics, 2025, 225–246, DOI: 10.1016/B978-0-443-15779-0.00006-7.
74. Y. Liu, et al., Machine learning based workflow for (micro)plastic spectral reconstruction and classification, Chemosphere, 2024, 369, 143835, DOI: 10.1016/j.chemosphere.2024.143835.

View Article Online
DOI: 10.1039/D5EN01084E

75. F. Herb, et al., Machine learning outperforms humans in microplastic characterization and reveals human labelling errors in FTIR data, J. Hazard. Mater., 2025, 487, 136989, DOI: 10.1016/j.jhazmat.2024.136989.
76. H. Li, et al., Deep learning assisted ATR-FTIR and Raman spectroscopy fusion technology for microplastic identification, Microchem. J., 2025, 212, 113224, DOI: 10.1016/j.microc.2025.113224.
77. X. Tian, et al., Quantum cascade laser imaging (LDIR) and machine learning for the identification of environmentally exposed microplastics and polymers, Environ. Res., 2022, 212, 113569, DOI: 10.1016/j.envres.2022.113569.
78. L. Xie, et al., Automatic identification of individual nanoplastics by Raman spectroscopy based on machine learning, Environ. Sci. Technol., 2023, 57, 46, 18203–18214, DOI: 10.1021/acs.est.3c03210.
79. L. Gong, et al., Machine learning-driven optical microfiltration device for improved nanoplastic sampling and detection in water systems, J. Hazard. Mater., 2025, 494, 138472, DOI: 10.1016/j.jhazmat.2025.138472.
80. C. Vitali, et al., Quantitative image analysis of microplastics in bottled water using artificial intelligence, Talanta, 2024, 266, 124965, DOI: 10.1016/j.talanta.2023.124965.
81. N. Meyers, et al., From microplastics to pixels: testing the robustness of two machine learning approaches for automated, Nile red-based marine microplastic identification, Environ. Sci. Pollut. Res., 2024, 31, 52, 61860–61875, DOI: 10.1007/s11356-024-35289-0.
82. N. Merlemis, et al., Laser induced fluorescence and machine learning: a novel approach to microplastic identification, Appl. Phys. B, 2024, 130, 9, 168, DOI: 10.1007/s00340-024-08308-8.
83. H. Ye, et al., Cost-effective and wireless portable device for rapid and sensitive quantification of micro/nanoplastics, ACS Sens., 2024, 9, 9, 4662–4670, DOI: 10.1021/acssensors.4c00957.
84. K. Han, et al., Innovative methods for microplastic characterization and detection: deep learning supported by photoacoustic imaging and automated pre-processing data, J. Environ. Manage., 2024, 359, 120954, DOI: 10.1016/j.jenvman.2024.120954.
85. Y. Su, et al., Lensless shadow microscopy-based shortcut analysis strategy for fast quantification of microplastic fibers released to water, Water Res., 2024, 258, 121758, DOI: 10.1016/j.watres.2024.121758.
86. J. W. Jeon, et al., Machine learning-integrated droplet microfluidic system for accurate quantification and classification of microplastics, Water Res., 2025, 274, 123161, DOI: 10.1016/j.watres.2025.123161.
87. J. S. Stine, et al., A novel approach for identifying nanoplastics by assessing deformation behavior with scanning electron microscopy, Micromachines (Basel), 2023, 14, 10, 1903, DOI: 10.3390/mi14101903.
88. S. Hasegawa, et al., Identification of polymeric nanoparticles using strategic peptide sensor configurations and machine learning, ACS Sens., 2025, 10, 7, 5036–5046, DOI: 10.1021/acssensors.5c01000.
89. M. Seggio, et al., Toward nano- and microplastic sensors: identification of nano- and microplastic particles via artificial intelligence combined with a plasmonic probe

View Article Online
DOI: 10.1039/D5EN01084E

functionalized with an estrogen receptor, ACS Omega, 2024, 9, 17, 18984–18994, DOI: 10.1021/acsomega.3c09485.
90. T. P. Forbes, et al., Rapid chemical screening of microplastics and nanoplastics by thermal desorption and pyrolysis mass spectrometry with unsupervised fuzzy clustering, Anal. Chem., 2023, 95, 33, 12373–12382, DOI: 10.1021/acs.analchem.3c01897.
91. H. Issa, et al., Modeling and numerical simulations of Brownian rodlike particles with anisotropic translational diffusion, Phys. Rev. Fluids, 2023, 8, 3, 033302, DOI: 10.1103/PhysRevFluids.8.033302.
92. T. Moodley, et al., Applications of mathematical modelling for assessing microplastic transport and fate in water environments: a comparative review, Environ. Monit. Assess., 2024, 196, 7, 667, DOI: 10.1007/s10661-024-12731-x.
93. C. Cai, et al., A review of methods for modeling microplastic transport in the marine environments, Mar. Pollut. Bull., 2023, 193, 115136, DOI: 10.1016/j.marpolbul.2023.115136.
94. L. D. Cuong, et al., Hydrodynamic modelling of microplastics transport in Bach Dang estuary, Vietnam J. Mar. Sci. Technol., 2022, 22, 4, 447–456, DOI: 10.15625/1859-3097/16490.
95. K. Pareta, 1D-2D hydrodynamic and sediment transport modelling using MIKE models, Discover Water, 2024, 4, 94, DOI: 10.1007/s43832-024-00130-9.
96. A. Pilechi, et al., A numerical framework for modeling fate and transport of microplastics in inland and coastal waters, Mar. Pollut. Bull., 2022, 184, 114119, DOI: 10.1016/j.marpolbul.2022.114119.
97. M. Ghazizadeh, et al., A high-performance ray tracing particle tracking model for the simulation of microplastics in inland and coastal aquatic environments, Comput. Phys. Commun., 2025, 307, 109423, DOI: 10.1016/j.cpc.2024.109423.
98. N. Simantiris, et al., Simulation of the transport of marine microplastic particles in the Ionian Archipelago (NE Ionian Sea) using a Lagrangian model and the control mechanisms affecting their transport, J. Hazard. Mater., 2022, 437, 129349, DOI: 10.1016/j.jhazmat.2022.129349.
99. S. Zhao, et al., The distribution of subsurface microplastics in the ocean, Nature, 2025, 641, 8061, 51–61, DOI: 10.1038/s41586-025-08818-1.
100. K. Senathirajah and C. Pattiaratchi, Microplastics in bays: transport processes and numerical models, Sci. Total Environ., 2025, 993, 179995, DOI: 10.1016/j.scitotenv.2025.179995.
101. N. Portillo De Arbeloa and A. Marzadri, Modeling microplastic dynamics in riverine systems: fate and transport analysis, Environ. Sci. Pollut. Res. Int., 2025, 32, 34, 20659–20677, DOI: 10.1007/s11356-025-36875-6.
102. M. Bigdeli, et al., Lagrangian modeling of marine microplastics fate and transport: the state of the science, J. Mar. Sci. Eng., 2022, 10, 4, 481, DOI: 10.3390/jmse10040481.
103. J. J. Armitage and S. Rohais, A numerical model of microplastic erosion, transport, and deposition for fluvial systems, Earth Surf. Dyn., 2025, 13, 4, 771–789, DOI: 10.5194/esurf-13-771-2025.

View Article Online
DOI: 10.1039/D5EN01084E

104. M. Martina and S. Trini Castelli, Modelling the potential long-range dispersion of atmospheric microplastics reaching a remote site, Atmos. Environ., 2023, 312, 120044, DOI: 10.1016/j.atmosenv.2023.120044.
105. E. Siht, et al., Modeling the pathways of microplastics in the Gulf of Finland, Baltic Sea – sensitivity of parametrizations, Ocean Dyn., 2024, 75, 9, DOI: 10.1007/s10236-024-01649-0.
106. R. Coyle, et al., Modeling microplastic transport in the marine environment: testing empirical models of particle terminal sinking velocity for irregularly shaped particles, ACS ES&T Water, 2023, 3, 4, 984–995, DOI: 10.1021/acsestwater.2c00466.
107. B. J. Kaimathuruthy, et al., Modelling microplastic dynamics in estuaries: a comprehensive review, challenges, and recommendations, Geosci. Model Dev., 2025, 18, 20, 7227–7255, DOI: 10.5194/gmd-18-7227-2025.
108. Y. Chen and Y. Wei, Unlocking subsurface microplastic dynamics: a perspective on modeling innovations, ACS ES&T Eng., 2024, 4, 12, 2852–2855, DOI: 10.1021/acsestengg.4c00663.
109. A. K. M. d. Oliveira, et al., Abiotic factors associated with microplastic pollution in surface water of a tropical estuary, Res. Soc. Dev., 2022, 11, 12, DOI: 10.33448/rsd-v11i12.34457.
110. M. George, et al., A threshold model of plastic waste fragmentation: new insights into the distribution of microplastics in the ocean and its evolution over time, Mar. Pollut. Bull., 2024, 199, 116012, DOI: 10.1016/j.marpolbul.2023.116012.
111. G. Giangeri, et al., Magnetite alters the metabolic interaction between methanogens and sulfate-reducing bacteria, Environ. Sci. Technol., 2023, 57, 43, 16399–16413, DOI: 10.1021/acs.est.3c05948.
112. B. J. Kaimathuruthy, et al., Modelling microplastic dynamics in estuaries: a comprehensive review, challenges and recommendations, Geosci. Model Dev., 2025, 18, 7227–7255, DOI: 10.5194/gmd-18-7227-2025.
113. I. Jalón-Rojas, et al., Effects of biofilms and particle physical properties on the rising and settling velocities of microplastic fibers and sheets, Environ. Sci. Technol., 2022, 56, 12, 8114–8123, DOI: 10.1021/acs.est.2c01302.
114. Y. Li, et al., Interactions between nano/micro plastics and suspended sediment in water: implications on aggregation and settling, Water Res., 2019, 161, 486–495, DOI: 10.1016/j.watres.2019.06.018.
115. O. S. Alimi, et al., Effects of weathering on the properties and fate of secondary microplastics from a polystyrene single-use cup, J. Hazard. Mater., 2023, 459, 131855, DOI: 10.1016/j.jhazmat.2023.131855.
116. F. Parrella, et al., Microplastics settling in turbid water: impacts of sediments-induced flow patterns on particle deposition rates, Environ. Sci. Technol., 2025, 59, 4, 2257–2265, DOI: 10.1021/acs.est.4c10551.
117. M. Mancini, et al., Suspended sediments mediate microplastic sedimentation in unidirectional flows, Sci. Total Environ., 2023, 890, 164363, DOI: 10.1016/j.scitotenv.2023.164363.

View Article Online
DOI: 10.1039/D5EN01084E

118. M. Molazadeh, et al., The role of turbulence in the deposition of intrinsically buoyant MPs, Sci. Total Environ., 2024, 911, 168540, DOI: 10.1016/j.scitotenv.2023.168540.
119. S. Ben, et al., Quantifying microplastic dispersion due to density effects, J. Hazard. Mater., 2024, 466, 133440, DOI: 10.1016/j.jhazmat.2024.133440.
120. M. Guo, et al., Microplastics in freshwater systems: dynamic behaviour and transport processes, Resour. Conserv. Recycl., 2024, 205, 107578, DOI: 10.1016/j.resconrec.2024.107578.
121. C. Ji, et al., Towards better predicting the settling velocity of film-shaped microplastics based on experiment and simulation data, Mar. Pollut. Bull., 2024, 203, 116493, DOI: 10.1016/j.marpolbul.2024.116493.
122. K. D. Goral, et al., Settling velocity of microplastic particles having regular and irregular shapes, Environ. Res., 2023, 228, 115783, DOI: 10.1016/j.envres.2023.115783.
123. J. Zhang and C. E. Choi, Improved settling velocity for microplastic fibers: a new shape-dependent drag model, Environ. Sci. Technol., 2022, 56, 2, 962–973, DOI: 10.1021/acs.est.1c06188.
124. X. Wang, et al., Impact of Fenton aging on the incipient motion of microplastic particles in open-channel flow, Sci. Total Environ., 2024, 953, 176220, DOI: 10.1016/j.scitotenv.2024.176220.
125. Z. Yu, et al., Investigation of the sheltering effects on the mobilization of microplastics in open-channel flow, Environ. Sci. Technol., 2023, 57, 30, 11259–11266, DOI: 10.1021/acs.est.3c02500.
126. K. D. Goral, et al., Shields diagram and the incipient motion of microplastic particles, Environ. Sci. Technol., 2023, 57, 25, 9362–9375, DOI: 10.1021/acs.est.3c02027.
127. F. Stábile, et al., Fate and biological uptake of polystyrene nanoparticles in freshwater wetland ecosystems, Environ. Sci.: Nano, 2024, 11, 8, 3475–3486, DOI: 10.1039/D3EN00628J.
128. Y. Xu, et al., Natural organic matter stabilizes pristine nanoplastics but destabilizes photochemical weathered nanoplastics in monovalent electrolyte solutions, Environ. Sci. Technol., 2025, 59, 3, 1822–1834, DOI: 10.1021/acs.est.4c11540.
129. D. Luo, et al., Photoaging-induced variations in heteroaggregation of nanoplastics and suspended sediments in aquatic environments: a case study on nanopolystyrene, Water Res., 2025, 268(Pt B), 122762, DOI: 10.1016/j.watres.2024.122762.
130. I. Suryana, et al., Systematic literature review for optimization system with advection–diffusion–reaction non-linear equation in water quality, IAENG Int. J. Appl. Math., 2024, 54, 12, 2541–2554.
131. F. Abdolahpur Monikh, et al., Importance of attachment efficiency in determining the fate of PS and PVC nanoplastic heteroaggregation with natural colloids using a multimedia model, Environ. Sci. Technol., 2025, 59, 9, 4674–4683, DOI: 10.1021/acs.est.4c10918.
132. H. Walch, et al., A versatile test system to determine nanomaterial heteroagglomeration attachment efficiency, Environ. Sci.: Nano, 2024, 11, 2, 588–600, DOI: 10.1039/D3EN00161J.

View Article Online
DOI: 10.1039/D5EN01084E

133. X. Liu, et al., Heteroaggregation of functionalized nanoplastics with Al_2O_3 particles in aquatic environments, Chem. Eng. J., 2025, 518, 164555, DOI: 10.1016/j.cej.2025.164555.
134. J. T. K. Quik, J. J. M. de Klein and A. A. Koelmans, Spatially explicit fate modelling of nanomaterials in natural waters, Water Res., 2015, 80, 200–208, DOI: 10.1016/j.watres.2015.05.025.
135. P. Domercq, A. Praetorius and M. MacLeod, The Full Multi: an open-source framework for modelling the transport and fate of nano- and microplastics in aquatic systems, Environ. Model. Softw., 2022, 148, 105291, DOI: 10.1016/j.envsoft.2021.105291.
136. J. A. J. Meesters, et al., Multimedia modeling of engineered nanoparticles with SimpleBox4nano: model definition and evaluation, Environ. Sci. Technol., 2014, 48, 10, 5726–5736, DOI: 10.1021/es500548h.
137. J. T. K. Quik, J. A. J. Meesters and A. A. Koelmans, A multimedia model to estimate the environmental fate of microplastic particles, Sci. Total Environ., 2023, 882, 163437, DOI: 10.1016/j.scitotenv.2023.163437.

View Article Online
DOI: 10.1039/D5EN01084E

Data Availability Statement

Data available upon reasonable request.